



ORIGINAL ARTICLE

Dynamics of omni-directional multi-rotor aerial vehicles, hexacopter as a case study



A.M. Shafei*, M.E. Yousefzadeh

Department of Mechanical Engineering, Shahid Bahonar University of Kerman, Kerman, Iran

Received 10 July 2024; accepted 22 January 2025

Available online 22 March 2025

KEYWORDS

Hexacopter;
Dynamic modelling;
Gibbs-Appell
formulation;
Trajectory tracking;
PD controller

Abstract This article presents a general formulation for the mathematical modeling of a specific class of aerial robots known as hexacopters. The mentioned robotic system, which consists of six arms with motors attached to each end, possesses a unique feature: it uses the minimum actuator required to reach a specific position in space with a defined orientation. To achieve this, it is vital to install the motors with an appropriate arrangement positioned at the end of each arm to ensure the robot's controllability. On the other hand, two virtual arms with zero lengths were used to describe the robot's orientation with regard to the inertial coordinate system in a tangible manner. One of the innovations carried out in this article is the standardization of the derivation of the motion equations of this robotic system procedure. For this purpose, first, the platform of the hexacopter is separated into several substructures. Following the previous step, the dynamic equations of each of these infrastructures are extracted in explicit form accordingly. Finally, the symbolic equations are merged, and as a result, the dynamic behavior of this aerial robot is formulated. The focus of this research is mainly on hexacopters. However, the presented method is generic enough to cover all aerial robots of this kind (with any number of arms and any relative arrangement between the members). Lastly, to show the robot's ability to reach a specific position in space with the desired orientation, the results of tracking a relatively complex trajectory by utilizing this robotic system are presented.

© 2025 The Authors. Publishing services by Elsevier B.V. on behalf of KeAi Communications Co. Ltd.

This is an open access article under the CC BY-NC-ND license (<http://creativecommons.org/licenses/by-nc-nd/4.0/>).

*Corresponding author.

E-mail address: shafei@uk.ac.ir (A.M. Shafei).

Peer review under the responsibility of Propulsion and Power Research.

1. Introduction

As a subset of multi-rotor unmanned aerial vehicles (UAVs), hexacopters can be used in a variety of applications through their unique capabilities, including vertical takeoff and landing, and agile maneuverability [1–6]. For instance, one can mention monitoring, aerial photography, high-altitude recording, search and rescue operations, and air transportation. The construction industry is one of the fields that has seen a growing use of hexacopters in recent years. Moreover, they are also utilized in agriculture and environmental supervision with indispensable popularity. The distinguishing characteristic of this specific type of aerial robots from other types, such as quadcopters and other multi-rotor UAVs, is the ability to fly with high stability in complicated aerial maneuvers. These robotic systems are increasing their popularity significantly, thanks to their ability to navigate challenging environments, which is an advantage in comparison with the other autonomous systems. Therefore, reaching a deep understanding of these hexacopters dynamics is crucial to enhance their performance in various operational scenarios. In other words, possessing the motion equations of these robotic systems allows researchers and engineers to have a better understanding of their flight and control characteristics, which will directly result in more efficient and stable development of robotic systems in this field.

As mentioned in the previous paragraph, hexacopters' dynamic analysis is vital in improving their performance. Research conducted so far has mainly focused on the effects of different hexacopter components on its movement characteristics. For instance, Zhang et al. [7] and Omari et al. [8] modeled the dynamics of hexacopters while taking into account the nonlinear effects caused by torques and forces generated by the motors. Park and Cho, in dynamic modeling, considered the effects of the components of this robotic system, including the platform, propellers, motors, and sensors in dynamic environments [9]. In the model introduced by Heidari and Saska, the effects of wind on the drone's passage were investigated. Furthermore, a modified potential field was included in this research to avoid obstacle collision [10]. Ghalamchi et al. investigated the vibrations produced by the structural defects of blades and their effects on the system dynamics [11]. In analyzing a hexacopter with an arm installed to its frame, Guo et al. investigated the alterations in the mass center of this robotic system by considering the coupling effects between the UAV and the mechanical arm [12]. Chen et al. developed a motion model by evaluating air density at different altitudes and estimating external torques [13]. Kamel et al. investigated a whole package mechatronics design of a tiltable-rotor aerial vehicle, named "Voliro", with narration in all subsequent sections, including mechanical design, mechatronics, dynamics, control, and implementation. However, the motion equations of this robotic system were presented in a non-recursive form [14]. Ye et al. studied the time delay factor in the dynamic equations of the hexacopter and its mounted robotic arm [15]. Moreover,

Arizaga et al. investigated the effects of suspended load fluctuations on the stability and control of a hexacopter with six rotors [16]. In research by Lee and Kim, the behavioral model of a hexacopter under various limited scenarios, such as motor torque limitation, rotation angle limitation, and working space limitation, were examined [17]. Guo et al. analyzed the dynamic behavior of a hexacopter with a passive manipulator mounted on its frame [18]. Among the other works carried out in this field, an honorable mention can be the design of a hexacopter by Giribet and Member, which has the capability of maintaining its balance in case of any of the motor's malfunctions, to the end that the thrust force does not suffer any significant decrease whatsoever [19]. In 2023, Angelis and Giulietti conducted a comprehensive study investigating the effects of cable-suspended loads on the hexacopter frame [20]. In 2024, Liang et al. with the help of a multimodal dynamic model, investigated the movement of a hexacopter in three-dimensional space with a six-axes robotic arm mounted on it [21]. The basis for deriving dynamic equations in the majority of past research is limited to Newton-Euler and Lagrange methods. Operation of the Newton-Euler method, in which calculations related to internal forces and torques are inevitable, is considered a complex and time-consuming matter for the current robotic system with a large number of constituent components. On the other hand, the main limitation of Lagrangian dynamics is the simultaneous application of partial and complete derivatives on the Lagrange function. The latter increases the complexity of extracting the motion equations when the degrees of freedom of such robotic systems increase. Another subject that has been neglected in most of the past works is the failure of implementing an automatic and systematic solution to derive the motion equations of this class of robotic systems. Therefore, it is necessary to review the dynamics of multi-rotor drones with a new approach.

A simple and straightforward dynamic method for determining the motive behavior of different mechanical systems, such as robots, is to use the Gibbs-Appell formulation. However, despite the numerous advantages of this method, it has not been the focus of robotic researchers when compared to the other approaches. The initial idea in this method was presented by Gibbs in 1879. Twenty years later, Appell expanded and developed Gibbs' idea and introduced a complete package known as "Gibbs-Appell Formulation". The primary advantage of the Gibbs-Appell formulation lies in the need for fewer mathematical computations than the other methods, such as Lagrange and Newton-Euler. This has made the Gibbs-Appell formulation a powerful tool for the dynamic analysis of mechanical systems. In the field of robotics, Shafei et al. have recently employed the above-mentioned technique in deriving the equations of motion of rigid and flexible mechanical arms [22–26], moving base robots [27–30], closed-loop mechanisms [31–34], and bipedal robotic systems [35–38]. Furthermore, by operating this method, Ahmadizadeh et al. studied the subject of collision without friction and collision with friction for multi-branch robots [39–42]. Nevertheless,

so far, there are no references available for obtaining the hexacopter's equations of motion using this technique. Therefore, one of the main goals of this article is to utilize this formulation in recursive form to derive the equations of motion of the hexacopter as a space robot.

In the field of aerial robots, it is crucial to design a controller to guide this type of robotic systems to track the desired trajectories. In this context, one can mention the trajectory tracking in the shape of "combined infinity", which is accomplished by a quadrotor using a robust adaptive controller [43]. The effect of factors such as load changes and wind blow on the performance of a quadcopter that benefits from the recursive sliding mode controller in trajectory tracking has been reported in Ref. [44]. The guidance of UAVs on straight lines and curved paths, including circles and ovals, using the PID and PD controllers has been analyzed in Ref. [45]. In the simulation conducted by Portillo et al. a Lyapunov function was implemented to ensure the stability of a single-rotor UAV while navigating a circular path with a radius of 5 m [46]. Drawing the word "ERU" with an octocopter and carrying out the same task by a dodecacopter using controllers such as PID and LQR are discussed in Ref. [47]. Using a PID controller, Park et al. developed an algorithm that prevented the accident of a hexacopter equipped with visual sensors [48]. Ferdous et al. solved the problem of collision with obstacles prevention for drones traveling near the ground surface using the Fuzzy controller [49]. According to the reports, mechanical failure in a six-rotor UAV is quite likely. Therefore, Colombo and Giribet depicted in another research that the ability to reset the rotors' angle can compensate for this kind of defects [50]. Another research conducted in this area is the second-order sliding mode controller designed by Ricardo and Santos, which successfully controlled a multi-rotor aerial robot in turbulent environments [51]. By reviewing the past research and studies, several points should be emphasized. The hexacopter's orientation, which tracks the desired trajectory, has not been the subject of these investigations. Moreover, due to the oversimplification of the dynamic model, authors have often used robust and sometimes complex controllers to compensate for this restriction. On the other hand, most of the desired paths defined for the movement of this class of aerial robots are limited to planar routes.

The primary objective of this research is a comprehensive and accurate study of the dynamics governing the movement of hexacopters. Thus, to the best of the authors' knowledge, the following are considered the innovations of this research:

- Deriving the equations of motion of hexacopters using the recursive Gibbs-Appell formulation to be easily extended to multi-rotor aerial robots with more than six blades, including octocopters and dodecacopters.
- Providing a tangible method to describe the orientation of the hexacopter relative to the inertial coordinate system by adding two virtual links with zero length and mass to the entire system.

- Kinematic and dynamic modeling of the constrained joints of the investigated robotic system in a fully systematic procedure to obtain constrained moments that their endurance is indispensable for maintaining the robot frame's integrity and coherence.
- Tracking the trajectory of the studied robotic systems in a way that takes into account the desired position and orientation simultaneously.

In this regard, the kinematic and dynamic equations of hexacopters are extracted in the second and third sections, respectively. In the fourth section, solving the system's inverse kinematics problem determines the generalized coordinates of the studied robotic system to achieve the defined and desired position and orientation. In the fifth section, the inverse dynamic equations are solved to obtain the thrust force generated by the motors, and the direct forward dynamic equations are solved to determine the system's response when these forces are applied. Finally, the sixth section presents the simulation results, and the seventh section depicts the findings of this study and the results.

2. Deriving the equations governing the hexacopters' kinematics

It is clear that a rigid body has six degrees of freedom in space (three translational degrees of freedom and three rotational degrees of freedom). As a result, it should be possible to control the movement of a body using six actuators that are properly installed on it. Figure 1 illustrates a rigid body consisting of six arms with a motor attached to the end point of each arm (shown with yellow). The shaft of each motor is connected to a propeller, and as the propeller rotates, a thrust force is produced along that shaft. The position of this rigid body (hereafter referred to as the hexacopter) is determined by having the position of only one of its points with respect to the inertial coordinate system $X_0Y_0Z_0$. In this research, the position of the first motor — whose distance from the X_0 , Y_0 , and Z_0 axes of the inertial coordinate system is equal to X_{O_1} , Y_{O_1} , and Z_{O_1} , respectively — has been employed for the mentioned calculation. On the other hand, it is more difficult to determine this rigid body's rotational position (orientation) with regard to the inertial coordinate system $X_0Y_0Z_0$. In this article, in order to express the orientation of this hexacopter more tangibly, two virtual arms with zero length and mass have been used. In Figure 1, these two arms labeled as *arm - 1* and *arm 0* are displayed in grey. Evidently, having the angles θ_{-1} , θ_0 , and θ_1 , the orientation of the first arm and, consequently, the orientation of the entire system relative to the inertial coordinate system can be determined. Based on the kinematic rules for robotic chains, which considers the rotation angle of each link relative to its adjacent link as a generalized coordinate, the hexacopter depicted in Figure 1 has eight rotational degrees of freedom (i.e., θ_i ; $i = -1, 0, \dots, 6$). However, due to the rigidity and symmetry of the platform of our robotic system, some of these generalized coordinates always have a fixed

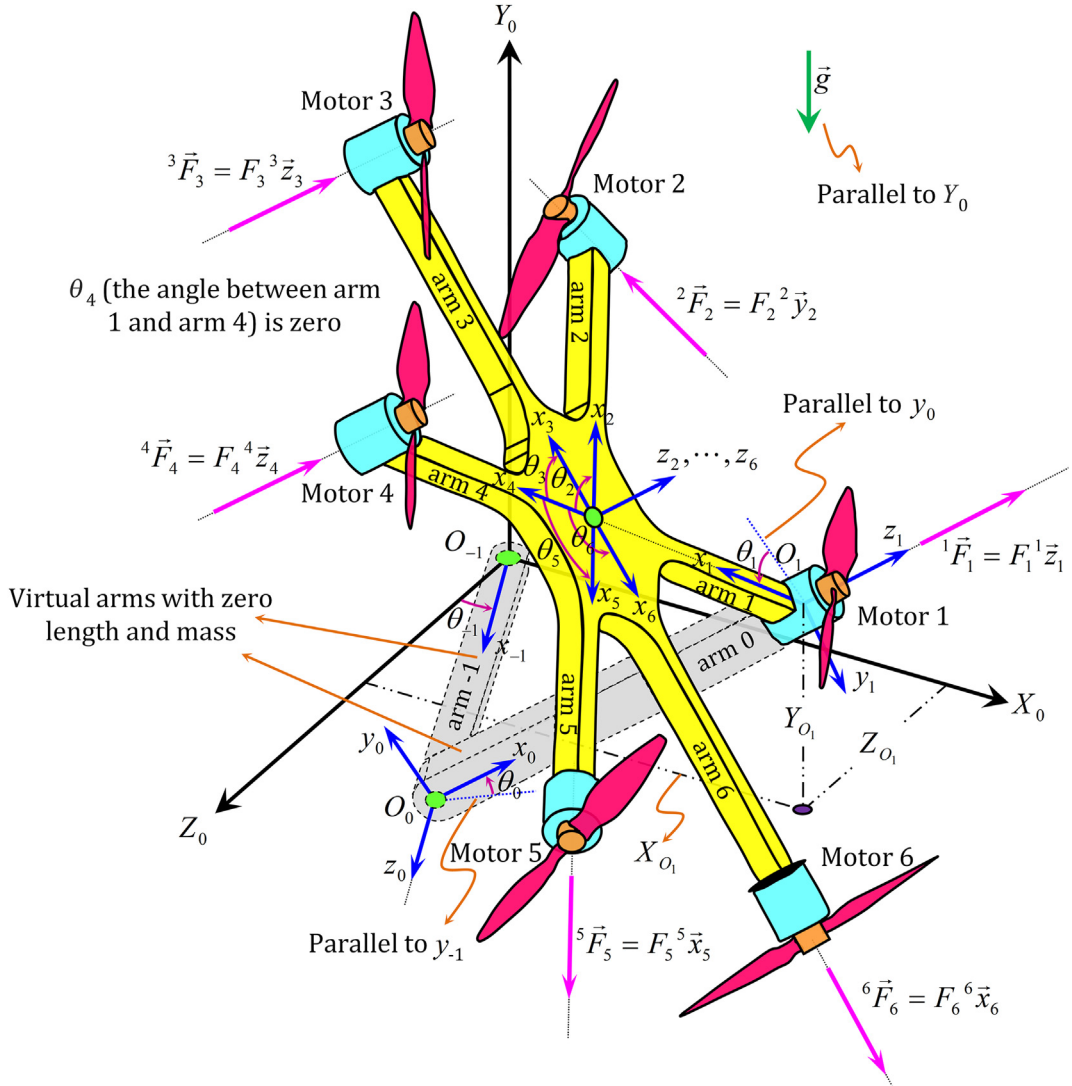


Figure 1 A hexacopter with a symmetrical platform and 60-degree angles between its arms.

value. For example, in Figure 1, the angles shown on the hexacopter's platform always have the constant values of $\theta_2 = -120^\circ$, $\theta_3 = -60^\circ$, $\theta_4 = 0^\circ$, $\theta_5 = +60^\circ$, and $\theta_6 = +120^\circ$.

For the dynamic analysis of this hexacopter, it is preferable to split it into a system consisting of several open kinematic chains. According to the division method presented in this paper, each chain starts from the O_{-1} joint, travels through the platform's center, and ends at one of the motors installed at the end of each arm. Therefore, the above system is divided into 5 chains, each of which is composed of 4 arms, as follows:

- chain 1: arm $-1 \rightarrow$ arm 0 \rightarrow arm 1 \rightarrow arm 2
- chain 2: arm $-1 \rightarrow$ arm 0 \rightarrow arm 1 \rightarrow arm 3
- chain 3: arm $-1 \rightarrow$ arm 0 \rightarrow arm 1 \rightarrow arm 4
- chain 4: arm $-1 \rightarrow$ arm 0 \rightarrow arm 1 \rightarrow arm 5
- chain 5: arm $-1 \rightarrow$ arm 0 \rightarrow arm 1 \rightarrow arm 6

These five chains are depicted in Figure 2. As observed in the figure, the first and second links in all these five chains are

illustrated with dashed lines. Because, as was noted before, these two links are virtual and have been added to the main system only to determine the orientation of the hexacopter with respect to the inertial coordinate system. On the other hand, excluding the first chain, the third link in other chains is also drawn with dashed lines; since the weight of this link is accounted for at its initial appearance inside the first chain. Therefore, its weight in other chains should be assumed zero. Another mentionable fact of this figure is the systematic and organized naming of the joints, their rotation angle, and the coordinate system assigned to each link. This nomenclature makes use of two subscripts. The first subscript indicates the chain number in which that joint or coordinate system is located ($j = 1, \dots, 5$); while, the second subscript indicates the joint number in that chain ($i = 1, \dots, 5$). According to this nomenclature, an angle like $\theta_{3,4}$ represents the rotation angle of the fourth link in the third chain. The last vital matter in this figure is the thrust force created by the propellers. Figure 1 illustrates how the first motor, located at the starting point of the first arm, is in the path of each of the five chains. However, its effect is

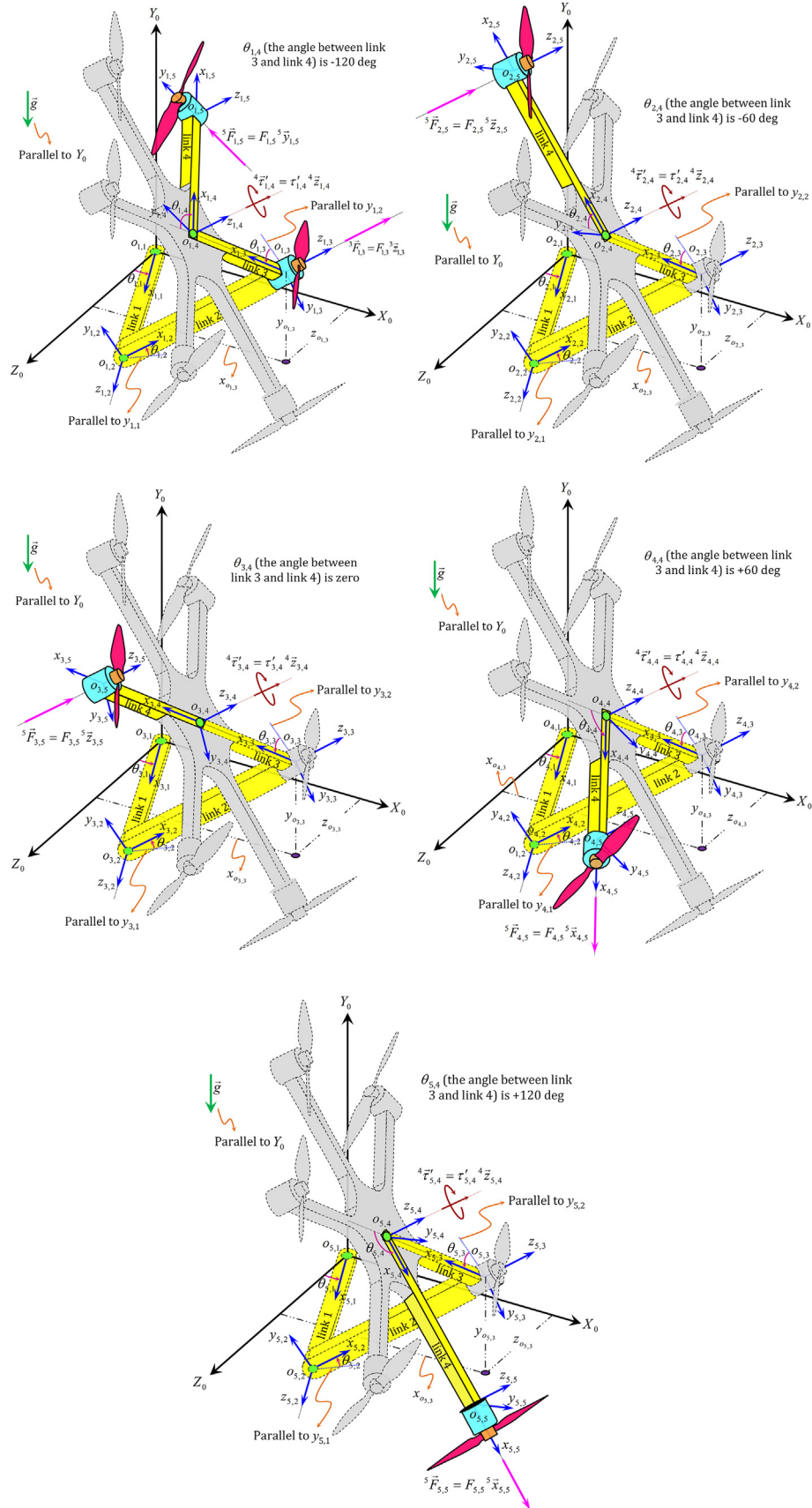


Figure 2 The hexacopter depicted in Figure 1 is partitioned into five distinct open kinematic chains.

$\frac{\partial x_{o_{j,i}}}{\partial \theta_{j,1}}$	$\frac{\partial x_{o_{j,i}}}{\partial \theta_{j,2}}$	$\frac{\partial x_{o_{j,i}}}{\partial \theta_{j,3}}$	$\frac{\partial x_{o_{j,i}}}{\partial \theta_{j,4}}$	$\frac{\partial x_{o_{j,i}}}{\partial x_{o_{j,3}}}$	$\frac{\partial x_{o_{j,i}}}{\partial y_{o_{j,3}}}$	$\frac{\partial x_{o_{j,i}}}{\partial z_{o_{j,3}}}$	$n = 1$
$\frac{\partial y_{o_{j,i}}}{\partial \theta_{j,1}}$	$\frac{\partial y_{o_{j,i}}}{\partial \theta_{j,2}}$	$\frac{\partial y_{o_{j,i}}}{\partial \theta_{j,3}}$	$\frac{\partial y_{o_{j,i}}}{\partial \theta_{j,4}}$	$\frac{\partial y_{o_{j,i}}}{\partial x_{o_{j,3}}}$	$\frac{\partial y_{o_{j,i}}}{\partial y_{o_{j,3}}}$	$\frac{\partial y_{o_{j,i}}}{\partial z_{o_{j,3}}}$	$n = 2$
$\frac{\partial z_{o_{j,i}}}{\partial \theta_{j,1}}$	$\frac{\partial z_{o_{j,i}}}{\partial \theta_{j,2}}$	$\frac{\partial z_{o_{j,i}}}{\partial \theta_{j,3}}$	$\frac{\partial z_{o_{j,i}}}{\partial \theta_{j,4}}$	$\frac{\partial z_{o_{j,i}}}{\partial x_{o_{j,3}}}$	$\frac{\partial z_{o_{j,i}}}{\partial y_{o_{j,3}}}$	$\frac{\partial z_{o_{j,i}}}{\partial z_{o_{j,3}}}$	$n = 3$
$m = 1$	$m = 2$	$m = 3$	$m = 4$	$m = 5$	$m = 6$	$m = 7$	

Figure 3 The Jacobian matrix of the i^{th} joint located in the j^{th} chain.

considered only in the first chain, and in the other chains, it is drawn passively (in grey) (Figure 2). This is because the thrust force of each motor should be counted only once in the dynamic computations. This issue is explained in more detail in the section related to generalized forces.

Before dealing with the dynamic equations of these five chains, it is necessary to calculate the Jacobian matrix of the joints affected by the propellers' thrust force. Suppose the position vector of the i^{th} joint in the j^{th} chain, expressed in the inertial coordinate system $X_0Y_0Z_0$, is indicated as ${}^0\vec{r}_{o_{j,i}} = \{x_{o_{j,i}} \ y_{o_{j,i}} \ z_{o_{j,i}}\}^T$, and the generalized coordinates of the j^{th} chain are represented by the vector $\vec{\Theta}_j = \{\theta_{j,1} \ \theta_{j,2} \ \theta_{j,3} \ \theta_{j,4} \ x_{o_{j,3}} \ y_{o_{j,3}} \ z_{o_{j,3}}\}^T$. In that case, the Jacobian matrix of this joint may be obtained using Figure 3. This matrix will be used in Section 3, where the discussion related to the modeling of constrained joints is presented.

3. Deriving the equations governing the hexacopters' dynamic

In the preceding section, the hexacopter structure was split into five open kinematic chains. We now seek to derive the equations of motion for these chains. Given that the approach utilized in this article relies on the Gibbs-Appell formulation, it is necessary to obtain the acceleration energy for these open kinematic chains. Previously, Shafei and Shafei extracted the acceleration energy of the i^{th} link in the j^{th} chain, whose base was able to move freely in space, using the following equation [52]:

$$\begin{aligned}
 S_{j,i} = & \frac{1}{2} B_{j,0i} {}^i\ddot{\vec{r}}_{o_{j,i}}^T \cdot {}^i\ddot{\vec{r}}_{o_{j,i}} \\
 & - {}^i\ddot{\vec{r}}_{o_{j,i}}^T \cdot B_{j,1i} {}^i\dot{\vec{\omega}}_{j,i} \\
 & - {}^i\ddot{\vec{r}}_{o_{j,i}}^T \cdot {}^i\tilde{\omega}_{j,i} B_{j,1i} {}^i\vec{\omega}_{j,i} \quad j = 1, \dots, 5 \\
 & + \frac{1}{2} {}^i\dot{\vec{\omega}}_{j,i}^T (B_{j,2i} + B_{j,3i}) {}^i\dot{\vec{\omega}}_{j,i} \quad i = 1, \dots, 4 \\
 & + {}^i\dot{\vec{\omega}}_{j,i}^T \cdot {}^i\tilde{\omega}_{j,i} (B_{j,2i} + B_{j,3i}) {}^i\vec{\omega}_{j,i} \\
 & + \text{ineffective terms}
 \end{aligned} \tag{1}$$

where the local coordinate system $x_{j,i}y_{j,i}z_{j,i}$ is used to express both ${}^i\dot{\vec{\omega}}_{j,i}$ and ${}^i\ddot{\vec{r}}_{o_{j,i}}$, representing the angular acceleration of the i^{th} link in the j^{th} chain and the linear acceleration of the i^{th} joint in the j^{th} chain, respectively. Furthermore, throughout this article, the symbol \sim on a vector denotes the skew-symmetric matrix associated with that vector. It should be noted that the constants $B_{j,0i}$, $B_{j,1i}$, $B_{j,2i}$, and $B_{j,3i}$ in Eq. (1) are introduced as follows:

$$B_{j,0i} = \int_0^{l_{j,i}} \mu_{j,i} d\eta_{j,i} \tag{2}$$

$$B_{j,1i} = \int_0^{l_{j,i}} \mu_{j,i} {}^i\tilde{\vec{r}}_{Q_{j,i}/o_{j,i}} d\eta_{j,i} \tag{3}$$

$$B_{j,2i} = \int_0^{l_{j,i}} \mu_{j,i} {}^i\vec{r}_{Q_{j,i}/o_{j,i}}^T {}^i\tilde{\vec{r}}_{Q_{j,i}/o_{j,i}} d\eta_{j,i} \tag{4}$$

$$B_{j,3i} = \int_0^{l_{j,i}} I'_{j,i} d\eta_{j,i} \tag{5}$$

where all the parameters mentioned in Eqs. (2)–(5) are defined in Ref. [52]. By adding the acceleration energies of the four links in the five chains displayed in Figure 2, the acceleration energy of the hexacopter illustrated in Figure 1 is calculated as follows:

$$S = \sum_{j=1}^5 \sum_{i=1}^4 S_{j,i} \tag{6}$$

Using the Gibbs-Appell formulation, the following equation represents $5 \times 7 = 35$ second-order differential equations that govern the dynamic behavior of the links in the open kinematic chains shown in Figure 2.

$$\frac{\partial S}{\partial \vec{\Theta}_j} = \vec{Q}_j \quad j = 1, \dots, 5 \tag{7}$$

where \vec{Q}_j is the vector of generalized forces associated with the j^{th} kinematic chain. The left-hand side of Eq. (7), which represents the rate of change of acceleration energy with respect to generalized accelerations, is expressed using the following equations:

$$\begin{aligned}
\frac{\partial S}{\partial \ddot{\theta}_{j,i}} &= \sum_{k=i+1}^4 \frac{\partial^k \ddot{\vec{r}}_{o_{j,k}}^T}{\partial \ddot{\theta}_{j,i}} \cdot {}^k \vec{\mathfrak{F}}_{j,k} & j = 1, \dots, 5 \\
&+ \sum_{k=i}^4 \frac{\partial^k \dot{\vec{\omega}}_{j,k}^T}{\partial \ddot{\theta}_{j,i}} \cdot {}^k \vec{\mathfrak{R}}_{j,k} & i = 1, \dots, 4 \\
\frac{\partial S}{\partial \ddot{x}_{o_{j,3}}} &= \sum_{k=1}^4 \frac{\partial^k \ddot{\vec{r}}_{o_{j,k}}^T}{\partial \ddot{x}_{o_{j,3}}} \cdot {}^k \vec{\mathfrak{F}}_{j,k} & j = 1, \dots, 5 \\
\frac{\partial S}{\partial \ddot{y}_{o_{j,3}}} &= \sum_{k=1}^4 \frac{\partial^k \ddot{\vec{r}}_{o_{j,k}}^T}{\partial \ddot{y}_{o_{j,3}}} \cdot {}^k \vec{\mathfrak{F}}_{j,k} & j = 1, \dots, 5 \\
\frac{\partial S}{\partial \ddot{z}_{o_{j,3}}} &= \sum_{k=1}^4 \frac{\partial^k \ddot{\vec{r}}_{o_{j,k}}^T}{\partial \ddot{z}_{o_{j,3}}} \cdot {}^k \vec{\mathfrak{F}}_{j,k} & j = 1, \dots, 5
\end{aligned} \tag{8}$$

where

$$\begin{aligned}
{}^k \vec{\mathfrak{F}}_{j,k} &= B_{j,0k} {}^k \ddot{\vec{r}}_{o_{j,k}} - B_{j,1k} {}^k \dot{\vec{\omega}}_{j,k} - {}^k \tilde{\omega}_{j,k} B_{j,1k} {}^k \vec{\omega}_{j,k} \\
{}^k \vec{\mathfrak{R}}_{j,k} &= B_{j,1k} {}^k \ddot{\vec{r}}_{o_{j,k}} + (B_{j,2k} + B_{j,3k}) {}^k \dot{\vec{\omega}}_{j,k} \\
&+ {}^k \tilde{\omega}_{j,k} (B_{j,2k} + B_{j,3k}) {}^k \vec{\omega}_{j,k}
\end{aligned} \tag{9}$$

The details on derivation of Eq. (8) can be found in Refs. [53,54]. Next, the right-hand side of Eq. (7) is examined, representing the vector of generalized forces. As shown in Figure 2, the thrust force ${}^i \vec{F}_{j,i}$ is applied to the i^{th} joint in the j^{th} chain, expressed in the local coordinate system of the same joint, i.e., $x_{j,i}, y_{j,i}, z_{j,i}$. In this article, it is assumed that the thrust force generated by the motors can only have a magnitude along one of the principal axes of the $x_{j,i}, y_{j,i}, z_{j,i}$ coordinate system. Thus, in order to demonstrate this force, a convention is presented here. According to this convention, we represent the thrust force as follows: ${}^i \vec{F}_{j,i} = F_{j,i} \vec{\vartheta}^1$ for a thrust force along the ${}^i \vec{x}_{j,i} = \{1 \ 0 \ 0\}^T$ axis, ${}^i \vec{F}_{j,i} = F_{j,i} \vec{\vartheta}^2$ for a thrust force along the ${}^i \vec{y}_{j,i} = \{0 \ 1 \ 0\}^T$ axis, and ${}^i \vec{F}_{j,i} = F_{j,i} \vec{\vartheta}^3$ for a thrust force along the ${}^i \vec{z}_{j,i} = \{0 \ 0 \ 1\}^T$ axis. Thus, this force can be represented in its most general form as ${}^i \vec{F}_{j,i} = F_{j,i} \vec{\vartheta}^k$; $k = 1$ or 2 or 3 .

In order to have a coherent and integrated hexacopter, like the one that is the subject of this investigation, it is necessary that some of its joints possess no rotational movement. For instance, in the hexacopter shown in Figure 1, there should be no rotational movement between the constituent arms. This necessitates that the joints $o_{1,4}$ through $o_{5,4}$ consistently adopt fixed angles of $\theta_{1,4} = -120^\circ$, $\theta_{2,4} = -60^\circ$, $\theta_{3,4} = 0^\circ$, $\theta_{4,4} = +60^\circ$, and $\theta_{5,4} = +120^\circ$, respectively (Figure 2). As a result, the constrained joint of each chain

($o_{j,4}; j = 1, \dots, 5$) experiences a constraint torque. This torque is represented in Figure 2 by the ${}^4 \vec{\tau}'_{j,4} = \tau'_{j,4} {}^4 \vec{z}_{j,4}$; $j = 1, \dots, 5$ notation (in fact, the prime symbol is used to emphasize that, in this case, we are dealing with a constraint rather than an active torque). Afterwards, the virtual work in the j^{th} branch, resulting from the active thrust force of the motors and the constraint torque of the platform, is presented as follows:

$$\delta W_j = \begin{cases} \delta^0 \vec{r}_{o_{j,3}}^T \cdot {}^0 \vec{F}_{j,3} + \delta^0 \vec{r}_{o_{j,5}}^T \cdot {}^0 \vec{F}_{j,5} + \delta \vec{\Theta}_j \cdot \vec{\tau}'_j & j = 1 \\ \delta^0 \vec{r}_{o_{j,5}}^T \cdot {}^0 \vec{F}_{j,5} + \delta \vec{\Theta}_j \cdot \vec{\tau}'_j & j = 2, \dots, 5 \end{cases} \tag{10}$$

It should be noted in Eq. (10) that, in contrast to other chains, the first chain possesses two thrust forces (Figure 2). On the other hand, the terms constituting the virtual work of the constraint torques in Eq. (10) are as follows:

$$\begin{aligned}
\delta \vec{\Theta}_j &= \{ \delta \theta_{j,1} \ \delta \theta_{j,2} \ \delta \theta_{j,3} \ \delta \theta_{j,4} \ \delta x_{o_{j,3}} \ \delta y_{o_{j,3}} \ \delta z_{o_{j,3}} \ }^T \\
\vec{\tau}'_j &= \{ 0 \ 0 \ 0 \ 1 \ 0 \ 0 \ 0 \ }^T \tau'_{j,4} = \vec{\varsigma}_j \tau'_{j,4} \quad j = 1, \dots, 5
\end{aligned} \tag{11}$$

Using the Jacobian matrix $J_{j,i}(\vec{\Theta}_j)$, the variations in the Cartesian space are related to the variations in the joint space by the equation $\delta^0 \vec{r}_{o_{j,i}} = J_{j,i} \delta \vec{\Theta}_j$. Additionally, the rotation matrix ${}^0 R_{j,i}$ can be employed to express the thrust force of the motors from the local coordinate system $x_{j,i}, y_{j,i}, z_{j,i}$ to the inertia coordinate system $X_0 Y_0 Z_0$, using the equation ${}^0 \vec{F}_{j,i} = {}^0 R_{j,i} {}^i \vec{F}_{j,i}$. By substituting these two relations, as well as Eq. (11), into Eq. (10), we get

$$\delta W_j = \begin{cases} \delta \vec{\Theta}_j^T \cdot \left[\begin{array}{l} \left(J_{j,3}^T {}^0 R_{j,3} \vec{\vartheta}^3 \right) F_{j,3} \\ + \left(J_{j,5}^T {}^0 R_{j,5} \vec{\vartheta}^2 \right) F_{j,5} \\ + \left(\vec{\varsigma}_j \right) \tau'_{j,4} \end{array} \right] & j = 1 \\ \delta \vec{\Theta}_j^T \cdot \left[\begin{array}{l} \left(J_{j,5}^T {}^0 R_{j,5} \vec{\vartheta}^k \right) F_{j,5} \\ + \left(\vec{\varsigma}_j \right) \tau'_{j,4} \end{array} \right] & j = 2, \dots, 5 \end{cases} \tag{12}$$

Note that the convention suggested for demonstrating the thrust force of the motors has been applied in the derivation of Eq. (12). The expression in brackets on the first line of Eq. (12) represents the vector of generalized forces of the first chain (\vec{Q}_1), while the expression in brackets on the

second line of Eq. (12) indicates the vector of generalized forces associated with the second through fifth chains ($\vec{Q}_j; j=2, \dots, 5$). It should be mentioned that the virtual work resulting from the earth's gravity is taken into account without any further calculations and only by applying the acceleration of $1\vec{g}$ to the base of each chain in the Y_0 direction [55].

Eq. (7) should be rewritten for computer simulations. To accomplish this goal, any terms with generalized accelerations $\ddot{\theta}_{j,i}$, $\ddot{x}_{o_{j,3}}$, $\ddot{y}_{o_{j,3}}$, and $\ddot{z}_{o_{j,3}}$, as well as those with constraint moments $\tau'_{j,4}$, should be transferred to the left side of the motion equations, while the residual terms that do not have the aforementioned characteristics should be moved to the right side. As a result, the equations of motion in the direct dynamic form can be represented as follows:

$$I_j(\vec{\Theta}_j) \ddot{\vec{\Theta}}_j - \vec{\varsigma}_j \tau'_{j,4} = \vec{R}_j(\vec{\Theta}_j, \dot{\vec{\Theta}}_j) + \vec{F}_j \quad j=1, \dots, 5 \quad (13)$$

where $I_j(\vec{\Theta}_j)$ and $\vec{R}_j(\vec{\Theta}_j, \dot{\vec{\Theta}}_j)$ are, respectively, the inertia matrix and the vector of dynamic residual terms of the j^{th} open kinematic chain, whose base has the ability to move freely in space. Furthermore, the vector \vec{F}_j represents the active generalized forces that are exerted on the system. This vector can be expressed as follows:

$$\vec{F}_j = \begin{cases} \begin{bmatrix} \vec{\Psi}_{j,3}^3 & \vec{\Psi}_{j,5}^2 \end{bmatrix} \begin{Bmatrix} F_{j,3} \\ F_{j,5} \end{Bmatrix} & j=1 \\ \vec{\Psi}_{j,5}^k F_{j,5} & j=2, \dots, 5 \end{cases} \quad (14)$$

where

$$\vec{\Psi}_{j,i}^k = J_{j,i}^T R_{j,i} \vec{\vartheta}^k \quad (15)$$

Eq. (13) for each chain consists of 7 second-order differential equations. These equations encompass four equations that pertain to the rotational movement of the joints in the chain, as well as three equations that pertain to the translational motion of the base of that chain. However, there are eight unknowns in total. These unknowns include four generalized rotational coordinates $\theta_{j,i}; i = 1, \dots, 4$, three generalized translational coordinates $x_{o_{j,3}}, y_{o_{j,3}}$, and $z_{o_{j,3}}$, and a constraint torque $\tau'_{j,4}$ applied to the constrained joint $o_{j,4}$. To solve for the unknown variables, it is required to use an auxiliary equation. This equation is obtained from the fact that the angular acceleration of the constrained joint in each chain is zero. Hence it gives:

$$\ddot{\theta}_{j,4} = 0 \Rightarrow \vec{\varsigma}_j^T \cdot \ddot{\vec{\Theta}}_j = 0 \quad j=1, \dots, 5 \quad (16)$$

Now, the direct dynamic equations for the five chains depicted in Figure 2 can be obtained by combining Eqs. (13) and (16) as follows:

$$\underbrace{\begin{bmatrix} I_j(\vec{\Theta}_j) & -\vec{\varsigma}_j \\ \vec{\varsigma}_j^T & 0 \end{bmatrix}}_{J_j^C} \underbrace{\begin{Bmatrix} \ddot{\vec{\Theta}}_j \\ \tau'_{j,4} \end{Bmatrix}}_{\ddot{\vec{\Theta}}_j^C} = \underbrace{\begin{Bmatrix} \vec{R}_j(\vec{\Theta}_j, \dot{\vec{\Theta}}_j) \\ 0 \end{Bmatrix}}_{\vec{R}_j^C} + \underbrace{\begin{Bmatrix} \vec{F}_j \\ 0 \end{Bmatrix}}_{\vec{F}_j^C} \quad j=1, \dots, 5 \quad (17)$$

In the equation above, $I_j^C(\vec{\Theta}_j)$ and $\vec{R}_j^C(\vec{\Theta}_j, \dot{\vec{\Theta}}_j)$ are respectively the inertia matrix and the vector of dynamic residual terms of the j^{th} open kinematic chain, where, in addition to its base's ability to move freely in space, one of its joints is also limited such that it cannot rotate (joint $o_{j,4}$). In fact, superscript C is employed to highlight the fact that this chain is constrained. In addition, the vectors of generalized accelerations $\ddot{\vec{\Theta}}_j^C$ and generalized forces \vec{F}_j^C in Eq. (17) are introduced as follows:

$$\ddot{\vec{\Theta}}_j^C = \left\{ \ddot{\theta}_{j,1} \quad \ddot{\theta}_{j,2} \quad \ddot{\theta}_{j,3} \quad \ddot{\theta}_{j,4} \quad \ddot{x}_{o_{j,3}} \quad \ddot{y}_{o_{j,3}} \quad \ddot{z}_{o_{j,3}} \quad \tau'_{j,4} \right\}^T$$

$$\vec{F}_j^C = \begin{cases} \begin{bmatrix} \vec{\Psi}_{j,3}^3 & \vec{\Psi}_{j,5}^2 \\ 0 & 0 \end{bmatrix} \begin{Bmatrix} F_{j,3} \\ F_{j,5} \end{Bmatrix} & j=1 \\ \begin{bmatrix} \vec{\Psi}_{j,5}^k \\ 0 \end{bmatrix} F_{j,5} & j=2, \dots, 5 \end{cases} \quad (18)$$

Figures 4 and 5 represent Eq. (17) for the five chains shown in Figure 2 graphically, including the inertia matrix, the vector of residual dynamic terms, and the vector of generalized forces.

Next, the motion equations for the five chains, as given in Eq. (17), need to be coupled appropriately to get the equations of motion for the primary system, the hexacopter depicted in Figure 1, as the following equation.

$$I_H(\vec{\Theta}_H) \ddot{\vec{\Theta}}_H = \vec{R}_H(\vec{\Theta}_H, \dot{\vec{\Theta}}_H) + \vec{F}_H \quad (19)$$

where $I_H(\vec{\Theta}_H)$ is the inertia matrix of the main system, i.e., the hexacopter depicted in Figure 1, and \vec{R}_H and \vec{F}_H are the vectors of the dynamic residual terms and generalized forces acting on the system, respectively. It should be noticed that the subscript H in the constituent terms of the above equation emphasizes that these terms belong to the main system, i.e., the hexacopter. To accomplish the aforementioned objective, it is necessary to establish the relationship between each chain's generalized coordinates and the main system's generalized coordinates. By considering Figures 1

and 2, these relationships can be determined, as shown in Figure 6.

For instance, according to this figure, the generalized accelerations and constraint torque in the fourth chain are $\ddot{\theta}_{4,1}$, $\ddot{\theta}_{4,2}$, $\ddot{\theta}_{4,3}$, $\ddot{\theta}_{4,4}$, $\ddot{x}_{o_{4,3}}$, $\ddot{y}_{o_{4,3}}$, $\ddot{z}_{o_{4,3}}$, and $\tau'_{4,4}$. Nevertheless, the variables $\ddot{\theta}_{-1}$, $\ddot{\theta}_0$, $\ddot{\theta}_1$, $\ddot{\theta}_5$, \ddot{X}_{O_1} , \ddot{Y}_{O_1} , \ddot{Z}_{O_1} , and τ'_4 represent the equivalent of the mentioned generalized accelerations and constraint torque in the main system. These variables are located in the -1st, 0th, 1st, 5th, 7th, 8th, 9th, and 13th rows of the generalized acceleration vector of the hexacopter, i.e., $\vec{\Theta}_H$. As a result, the entries of this robotic chain's inertia matrix, I_4^C , must be inserted in the -1st, 0th, 1st, 5th, 7th, 8th, 9th, and 13th rows and columns of the hexacopter's inertia matrix, I_H . Upon executing this procedure for the other robotic chains, the hexacopter's inertia matrix is created, incorporating the dynamic coupling of each chain, as illustrated in Figure 7. Similarly, the vector representing the dynamic residual terms (i.e., \vec{R}_H) and the vector representing the generalized forces acting on this robotic system (i.e., \vec{F}_H) are constructed based on Figures 8 and 9, respectively.

It should be noted that the entry $I_{k,t}^j$ in the hexacopter's inertia matrix (Figure 7) is the same as the entry $I_j(k,t)$ in the inertia matrix of each chain (Figure 4), which is written in this way due to the lack of space. This issue is also true for the entries of the dynamic residual terms vector. In other words, we have $R_{k,1}^j = R_j(k,1)$. Furthermore, by comparing Figures 1 and 2, we can infer the following relationship between the thrust forces in the main system and the thrust forces in the chains, which has been used in constructing vector \vec{F}_H .

$I_1^C =$									
$\ddot{\theta}_{1,1}$	$\ddot{\theta}_{1,2}$	$\ddot{\theta}_{1,3}$	$\ddot{\theta}_{1,4}$	$\ddot{x}_{o_{1,3}}$	$\ddot{y}_{o_{1,3}}$	$\ddot{z}_{o_{1,3}}$	$\tau'_{1,4}$		
$I_1(1,1)$	$I_1(1,2)$	$I_1(1,3)$	$I_1(1,4)$	$I_1(1,5)$	$I_1(1,6)$	$I_1(1,7)$	0		
$I_1(2,2)$	$I_1(2,3)$	$I_1(2,4)$	$I_1(2,5)$	$I_1(2,6)$	$I_1(2,7)$	0			
$I_1(3,3)$	$I_1(3,4)$	$I_1(3,5)$	$I_1(3,6)$	$I_1(3,7)$	0				
	$I_1(4,4)$	$I_1(4,5)$	$I_1(4,6)$	$I_1(4,7)$	-1				
	$I_1(5,5)$	$I_1(5,6)$	$I_1(5,7)$	0					
	$I_1(6,6)$	$I_1(6,7)$	0						
		$I_1(7,7)$	0						
Symmetric									
0	0	0	1	0	0	0	0		
$t = -1$	$t = 0$	$t = 1$	$t = 2$	$t = 7$	$t = 8$	$t = 9$	$t = 10$		
$I_2^C =$									
$\ddot{\theta}_{2,1}$	$\ddot{\theta}_{2,2}$	$\ddot{\theta}_{2,3}$	$\ddot{\theta}_{2,4}$	$\ddot{x}_{o_{2,3}}$	$\ddot{y}_{o_{2,3}}$	$\ddot{z}_{o_{2,3}}$	$\tau'_{2,4}$		
$I_2(1,1)$	$I_2(1,2)$	$I_2(1,3)$	$I_2(1,4)$	$I_2(1,5)$	$I_2(1,6)$	$I_2(1,7)$	0		
$I_2(2,2)$	$I_2(2,3)$	$I_2(2,4)$	$I_2(2,5)$	$I_2(2,6)$	$I_2(2,7)$	0			
$I_2(3,3)$	$I_2(3,4)$	$I_2(3,5)$	$I_2(3,6)$	$I_2(3,7)$	0				
	$I_2(4,4)$	$I_2(4,5)$	$I_2(4,6)$	$I_2(4,7)$	-1				
	$I_2(5,5)$	$I_2(5,6)$	$I_2(5,7)$	0					
	$I_2(6,6)$	$I_2(6,7)$	0						
		$I_2(7,7)$	0						
Symmetric									
0	0	0	1	0	0	0	0		
$t = -1$	$t = 0$	$t = 1$	$t = 3$	$t = 7$	$t = 8$	$t = 9$	$t = 11$		
$I_3^C =$									
$\ddot{\theta}_{3,1}$	$\ddot{\theta}_{3,2}$	$\ddot{\theta}_{3,3}$	$\ddot{\theta}_{3,4}$	$\ddot{x}_{o_{3,3}}$	$\ddot{y}_{o_{3,3}}$	$\ddot{z}_{o_{3,3}}$	$\tau'_{3,4}$		
$I_3(1,1)$	$I_3(1,2)$	$I_3(1,3)$	$I_3(1,4)$	$I_3(1,5)$	$I_3(1,6)$	$I_3(1,7)$	0		
$I_3(2,2)$	$I_3(2,3)$	$I_3(2,4)$	$I_3(2,5)$	$I_3(2,6)$	$I_3(2,7)$	0			
$I_3(3,3)$	$I_3(3,4)$	$I_3(3,5)$	$I_3(3,6)$	$I_3(3,7)$	0				
	$I_3(4,4)$	$I_3(4,5)$	$I_3(4,6)$	$I_3(4,7)$	-1				
	$I_3(5,5)$	$I_3(5,6)$	$I_3(5,7)$	0					
	$I_3(6,6)$	$I_3(6,7)$	0						
		$I_3(7,7)$	0						
Symmetric									
0	0	0	1	0	0	0	0		
$t = -1$	$t = 0$	$t = 1$	$t = 4$	$t = 7$	$t = 8$	$t = 9$	$t = 12$		
$I_4^C =$									
$\ddot{\theta}_{4,1}$	$\ddot{\theta}_{4,2}$	$\ddot{\theta}_{4,3}$	$\ddot{\theta}_{4,4}$	$\ddot{x}_{o_{4,3}}$	$\ddot{y}_{o_{4,3}}$	$\ddot{z}_{o_{4,3}}$	$\tau'_{4,4}$		
$I_4(1,1)$	$I_4(1,2)$	$I_4(1,3)$	$I_4(1,4)$	$I_4(1,5)$	$I_4(1,6)$	$I_4(1,7)$	0		
$I_4(2,2)$	$I_4(2,3)$	$I_4(2,4)$	$I_4(2,5)$	$I_4(2,6)$	$I_4(2,7)$	0			
$I_4(3,3)$	$I_4(3,4)$	$I_4(3,5)$	$I_4(3,6)$	$I_4(3,7)$	0				
	$I_4(4,4)$	$I_4(4,5)$	$I_4(4,6)$	$I_4(4,7)$	-1				
	$I_4(5,5)$	$I_4(5,6)$	$I_4(5,7)$	0					
	$I_4(6,6)$	$I_4(6,7)$	0						
		$I_4(7,7)$	0						
Symmetric									
0	0	0	1	0	0	0	0		
$t = -1$	$t = 0$	$t = 1$	$t = 5$	$t = 7$	$t = 8$	$t = 9$	$t = 13$		
$I_5^C =$									
$\ddot{\theta}_{5,1}$	$\ddot{\theta}_{5,2}$	$\ddot{\theta}_{5,3}$	$\ddot{\theta}_{5,4}$	$\ddot{x}_{o_{5,3}}$	$\ddot{y}_{o_{5,3}}$	$\ddot{z}_{o_{5,3}}$	$\tau'_{5,4}$		
$I_5(1,1)$	$I_5(1,2)$	$I_5(1,3)$	$I_5(1,4)$	$I_5(1,5)$	$I_5(1,6)$	$I_5(1,7)$	0		
$I_5(2,2)$	$I_5(2,3)$	$I_5(2,4)$	$I_5(2,5)$	$I_5(2,6)$	$I_5(2,7)$	0			
$I_5(3,3)$	$I_5(3,4)$	$I_5(3,5)$	$I_5(3,6)$	$I_5(3,7)$	0				
	$I_5(4,4)$	$I_5(4,5)$	$I_5(4,6)$	$I_5(4,7)$	-1				
	$I_5(5,5)$	$I_5(5,6)$	$I_5(5,7)$	0					
	$I_5(6,6)$	$I_5(6,7)$	0						
		$I_5(7,7)$	0						
Symmetric									
0	0	0	1	0	0	0	0		
$t = -1$	$t = 0$	$t = 1$	$t = 6$	$t = 7$	$t = 8$	$t = 9$	$t = 14$		

Figure 4 The inertia matrices for the five chains depicted in Figure 2.

$$\begin{aligned}\vec{F} &= \underbrace{\{F_1 F_2 F_3 F_4 F_5 F_6\}}_{{\text{Trust forces in the main system}}}^T \\ &= \underbrace{\{F_{1,3} F_{1,5} F_{2,5} F_{3,5} F_{4,5} F_{5,5}\}}_{{\text{Trust forces in the chains}}}^T\end{aligned}\quad (20)$$

Note that some parts of Figures 7 through 9 are labeled as matrix A (the first 11 rows and the first 11 columns of the inertial matrix I_H), matrix B (the first 11 rows and the last five columns of the inertial matrix I_H), matrix Ψ (the first 11 rows and all columns of the matrix appearing in the expression related to the generalized forces vector \vec{F}_H), and vector \vec{R}_H (the first 11 rows of the dynamic residual terms vector \vec{R}_H). Section 5 employs these matrices and vectors to solve the inverse dynamic problem.

4. Defining the desired position and orientation of the hexacopter under investigation

Before simulating the motion equations, it is necessary to define a desired trajectory for the studied robotic system. This desired trajectory should encompass two essential pieces of information. First, it determines the desired position of a specific point on the hexacopter relative to the inertial coordinate system. Second, the aforementioned robot's desired orientation with regard to the base coordinate system is known at all times.

Figure 1 displays five coordinate systems positioned at the center of the hexacopter. Each coordinate system is assigned to one of the hexacopter's arms based on the rules established by Denavit and Hartenberg. Once again,

$$\begin{aligned}
\vec{R}_1^C &= \begin{bmatrix} R_1(1,1) \\ R_1(2,1) \\ R_1(3,1) \\ R_1(4,1) \\ R_1(5,1) \\ R_1(6,1) \\ R_1(7,1) \\ 0 \end{bmatrix} & \vec{F}_1^C &= \begin{bmatrix} \Psi_{1,3}^3(1,1) & \Psi_{1,5}^2(1,1) \\ \Psi_{1,3}^3(2,1) & \Psi_{1,5}^2(2,1) \\ \Psi_{1,3}^3(3,1) & \Psi_{1,5}^2(3,1) \\ \Psi_{1,3}^3(4,1) & \Psi_{1,5}^2(4,1) \\ \Psi_{1,3}^3(5,1) & \Psi_{1,5}^2(5,1) \\ \Psi_{1,3}^3(6,1) & \Psi_{1,5}^2(6,1) \\ \Psi_{1,3}^3(7,1) & \Psi_{1,5}^2(7,1) \\ 0 & 0 \end{bmatrix} \times \begin{bmatrix} F_{1,3} \\ F_{1,5} \end{bmatrix} & k = -1 \\ & & & k = 0 \\ & & & k = 1 \\ & & & k = 2 \\ & & & k = 7 \\ & & & k = 8 \\ & & & k = 9 \\ & & & k = 10 \\ \\
\vec{R}_2^C &= \begin{bmatrix} R_2(1,1) \\ R_2(2,1) \\ R_2(3,1) \\ R_2(4,1) \\ R_2(5,1) \\ R_2(6,1) \\ R_2(7,1) \\ 0 \end{bmatrix} & \vec{F}_2^C &= \begin{bmatrix} \Psi_{2,5}^3(1,1) \\ \Psi_{2,5}^3(2,1) \\ \Psi_{2,5}^3(3,1) \\ \Psi_{2,5}^3(4,1) \\ \Psi_{2,5}^3(5,1) \\ \Psi_{2,5}^3(6,1) \\ \Psi_{2,5}^3(7,1) \\ 0 \end{bmatrix} \times \begin{bmatrix} F_{2,5} \end{bmatrix} & k = -1 \\ & & & k = 0 \\ & & & k = 1 \\ & & & k = 3 \\ & & & k = 7 \\ & & & k = 8 \\ & & & k = 9 \\ & & & k = 11 \\ \\
\vec{R}_3^C &= \begin{bmatrix} R_3(1,1) \\ R_3(2,1) \\ R_3(3,1) \\ R_3(4,1) \\ R_3(5,1) \\ R_3(6,1) \\ R_3(7,1) \\ 0 \end{bmatrix} & \vec{F}_3^C &= \begin{bmatrix} \Psi_{3,5}^3(1,1) \\ \Psi_{3,5}^3(2,1) \\ \Psi_{3,5}^3(3,1) \\ \Psi_{3,5}^3(4,1) \\ \Psi_{3,5}^3(5,1) \\ \Psi_{3,5}^3(6,1) \\ \Psi_{3,5}^3(7,1) \\ 0 \end{bmatrix} \times \begin{bmatrix} F_{3,5} \end{bmatrix} & k = -1 \\ & & & k = 0 \\ & & & k = 1 \\ & & & k = 4 \\ & & & k = 7 \\ & & & k = 8 \\ & & & k = 9 \\ & & & k = 12 \\ \\
\vec{R}_4^C &= \begin{bmatrix} R_4(1,1) \\ R_4(2,1) \\ R_4(3,1) \\ R_4(4,1) \\ R_4(5,1) \\ R_4(6,1) \\ R_4(7,1) \\ 0 \end{bmatrix} & \vec{F}_4^C &= \begin{bmatrix} \Psi_{4,5}^1(1,1) \\ \Psi_{4,5}^1(2,1) \\ \Psi_{4,5}^1(3,1) \\ \Psi_{4,5}^1(4,1) \\ \Psi_{4,5}^1(5,1) \\ \Psi_{4,5}^1(6,1) \\ \Psi_{4,5}^1(7,1) \\ 0 \end{bmatrix} \times \begin{bmatrix} F_{4,5} \end{bmatrix} & k = -1 \\ & & & k = 0 \\ & & & k = 1 \\ & & & k = 5 \\ & & & k = 7 \\ & & & k = 8 \\ & & & k = 9 \\ & & & k = 13 \\ \\
\vec{R}_5^C &= \begin{bmatrix} R_5(1,1) \\ R_5(2,1) \\ R_5(3,1) \\ R_5(4,1) \\ R_5(5,1) \\ R_5(6,1) \\ R_5(7,1) \\ 0 \end{bmatrix} & \vec{F}_5^C &= \begin{bmatrix} \Psi_{5,5}^1(1,1) \\ \Psi_{5,5}^1(2,1) \\ \Psi_{5,5}^1(3,1) \\ \Psi_{5,5}^1(4,1) \\ \Psi_{5,5}^1(5,1) \\ \Psi_{5,5}^1(6,1) \\ \Psi_{5,5}^1(7,1) \\ 0 \end{bmatrix} \times \begin{bmatrix} F_{5,5} \end{bmatrix} & k = -1 \\ & & & k = 0 \\ & & & k = 1 \\ & & & k = 6 \\ & & & k = 7 \\ & & & k = 8 \\ & & & k = 9 \\ & & & k = 14
\end{aligned}$$

Figure 5 The vectors of dynamic residual terms and generalized forces for the five chains depicted in Figure 2.

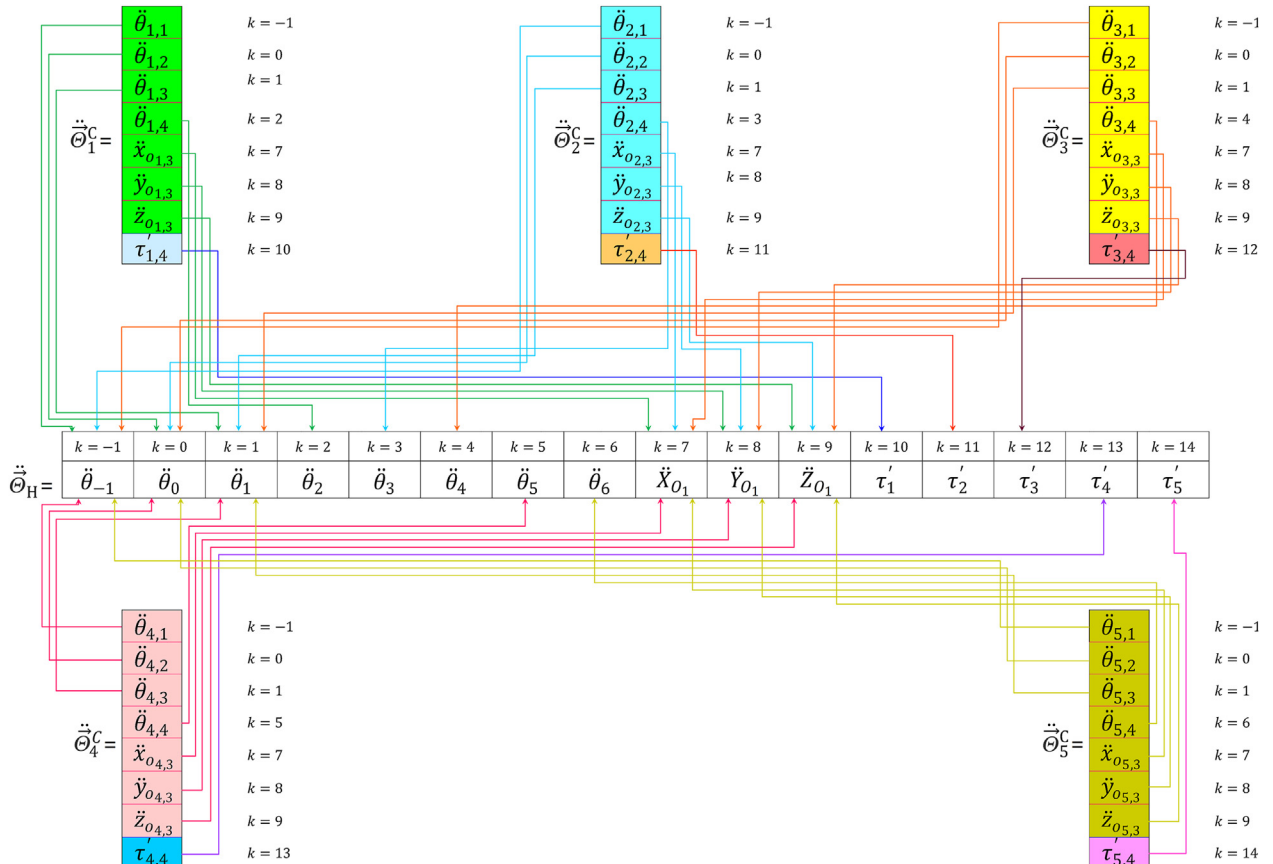


Figure 6 The relationship between the generalized accelerations and constraint torque of each chain and those in the main system.

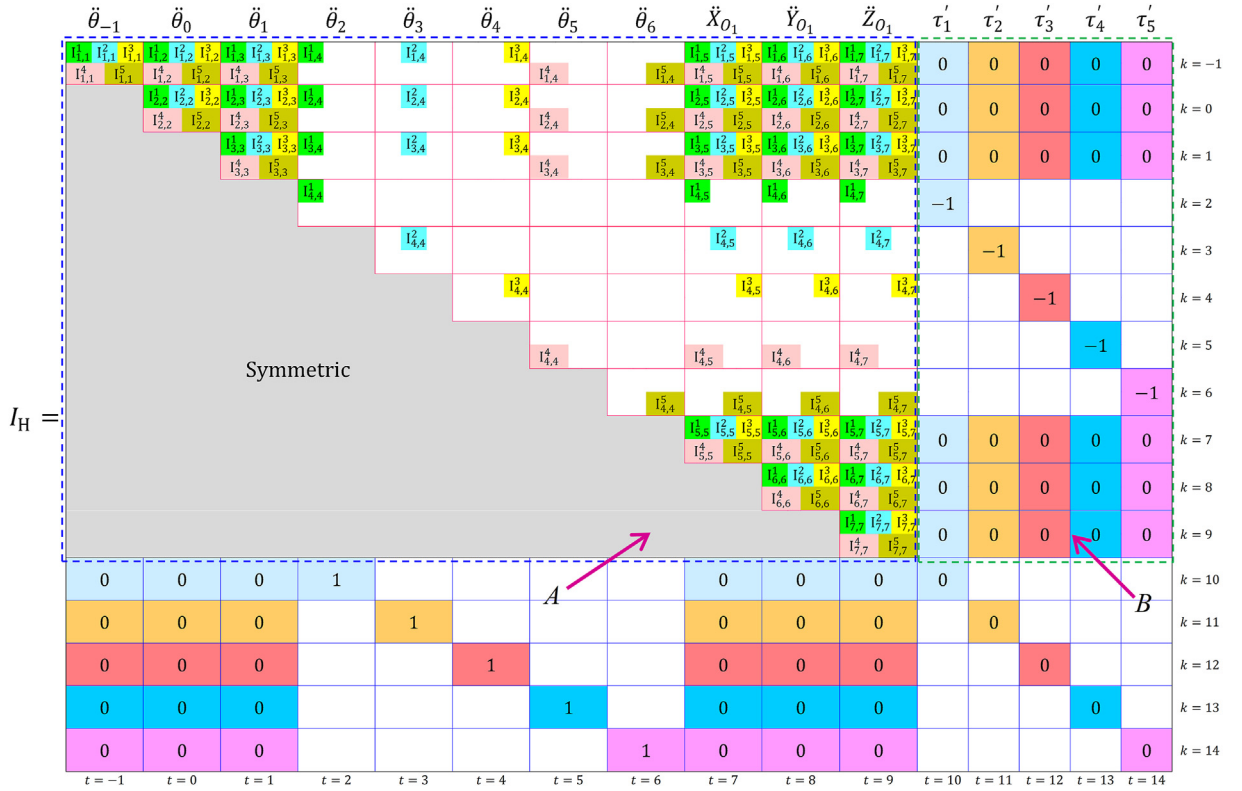


Figure 7 The hexacopter’s inertia matrix is developed by combining the chains’ inertia matrices shown in [Figure 4](#).

examining the coordinate system associated with the second arm in this figure. The origin of this coordinate system, O_2 , is exactly in the center of the hexacopter; the x_2 -axis is along the second arm, and the z_2 -axis is perpendicular to the hexacopter’s platform. Now, using this coordinate system, we establish the desired path of this robotic system based on the representation shown in [Figure 10](#). The desired trajectory is a path where the center of the hexacopter, i.e., O_2 , moves along the curve whose parametric equations are determined by the user ([Figure 10](#) displays this curve in blue). Furthermore, throughout this movement, it is necessary for the x_2 -axis to always be tangent to the curve aligned with the \vec{e}_t direction, the y_2 -axis to be perpendicular to the curve (in the direction of its curvature) aligned with the \vec{e}_n direction, and the z_2 -axis to be perpendicular to the robot’s platform and aligned with the \vec{e}_b direction. Therefore, we first need to derive expressions for the unit vectors \vec{e}_t , \vec{e}_n , and \vec{e}_b using the parametric equations that describe the desired trajectory of the hexacopter’s center. If the vector $\vec{r}_{O_2}(t) = X_{O_2}^d(t)\vec{I} + Y_{O_2}^d(t)\vec{J} + Z_{O_2}^d(t)\vec{K}$ represents the parametric equations of a desired path for the origin O_2 , using vector calculus, one can demonstrate that the unit tangent vector to this trajectory is given as follows:

$$\begin{aligned}\vec{e}_t(t) &= \frac{d^0 \vec{r}_{O_2}/dt}{\left| d^0 \vec{r}_{O_2}/dt \right|} = \frac{\dot{X}_{O_2}^d \vec{I} + \dot{Y}_{O_2}^d \vec{J} + \dot{Z}_{O_2}^d \vec{K}}{\left(\dot{X}_{O_2}^2 + \dot{Y}_{O_2}^2 + \dot{Z}_{O_2}^2 \right)^{\frac{1}{2}}} \\ &= \alpha_1(t)\vec{I} + \alpha_2(t)\vec{J} + \alpha_3(t)\vec{K}\end{aligned}\quad (21)$$

Furthermore, the unit vector perpendicular to the trajectory (towards the curve’s curvature) can be calculated as follows:

$$\begin{aligned}\vec{e}_n(t) &= \frac{d \vec{e}_t/dt}{\left| d \vec{e}_t/dt \right|} = \frac{\dot{\alpha}_1 \vec{I} + \dot{\alpha}_2 \vec{J} + \dot{\alpha}_3 \vec{K}}{(\dot{\alpha}_1^2 + \dot{\alpha}_2^2 + \dot{\alpha}_3^2)^{\frac{1}{2}}} \\ &= \beta_1(t)\vec{I} + \beta_2(t)\vec{J} + \beta_3(t)\vec{K}\end{aligned}\quad (22)$$

Now, having the directions \vec{e}_t and \vec{e}_n to establish a right-handed coordinate system, the unit vector \vec{e}_b perpendicular to the plane containing the vectors \vec{e}_t and \vec{e}_n is obtained as follows:

$$\vec{e}_b(t) = \frac{\vec{e}_t \times \vec{e}_n}{\left| \vec{e}_t \times \vec{e}_n \right|} = \gamma_1(t)\vec{I} + \gamma_2(t)\vec{J} + \gamma_3(t)\vec{K} \quad (23)$$

Therefore, the orientation of the coordinate system $e_t e_n e_b$ relative to the inertial coordinate system $X_0 Y_0 Z_0$ is obtained by the following rotation matrix:

$${}_{X_0 Y_0 Z_0} R_{e_t e_n e_b} = \begin{bmatrix} \alpha_1 & \beta_1 & \gamma_1 \\ \alpha_2 & \beta_2 & \gamma_2 \\ \alpha_3 & \beta_3 & \gamma_3 \end{bmatrix} \quad (24)$$

On the other hand, using rotation matrices, the orientation of the coordinate system $x_2 y_2 z_2$ with respect to the inertial coordinate system $X_0 Y_0 Z_0$ is obtained as follows:

$$\begin{aligned}
{}^{X_0Y_0Z_0}R_{x_2y_2z_2} &= {}^{X_0Y_0Z_0}R_{x_{-1}y_{-1}z_{-1}} {}^{x_{-1}y_{-1}z_{-1}}R_{x_0y_0z_0} {}^{x_0y_0z_0}R_{x_1y_1z_1} {}^{x_1y_1z_1}R_{x_2y_2z_2} \Rightarrow \\
{}^{X_0Y_0Z_0}R_{x_2y_2z_2} &= \begin{bmatrix} \sin \theta_{-1} \sin(\theta_1 + \theta_2) - \cos \theta_{-1} \sin \theta_0 \cos(\theta_1 + \theta_2) \\ \cos \theta_0 \cos(\theta_1 + \theta_2) \\ \cos \theta_{-1} \sin(\theta_1 + \theta_2) + \sin \theta_{-1} \sin \theta_0 \cos(\theta_1 + \theta_2) \\ \cos \theta_{-1} \sin \theta_0 \sin(\theta_1 + \theta_2) + \sin \theta_{-1} \cos(\theta_1 + \theta_2) & \cos \theta_{-1} \cos \theta_0 \\ -\cos \theta_0 \sin(\theta_1 + \theta_2) & \sin \theta_0 \\ \cos \theta_{-1} \cos(\theta_1 + \theta_2) - \sin \theta_{-1} \sin \theta_0 \sin(\theta_1 + \theta_2) & -\cos \theta_0 \sin \theta_{-1} \end{bmatrix} \quad (25)
\end{aligned}$$

$$\vec{R}_H = \begin{bmatrix} k = -1 & k = 0 & k = 1 & k = 2 & k = 3 & k = 4 & k = 5 & k = 6 & k = 7 & k = 8 & k = 9 & k = 10 & k = 11 & k = 12 & k = 13 & k = 14 & T \\ \begin{matrix} R_{1,1}^1, R_{1,1}^2, R_{1,1}^3, R_{2,1}^1, R_{2,1}^2, R_{2,1}^3, R_{3,1}^1, R_{3,1}^2, R_{3,1}^3, R_{4,1}^1 \\ R_{1,1}^4, R_{1,1}^5, R_{2,1}^4, R_{2,1}^5, R_{3,1}^4, R_{3,1}^5, R_{4,1}^4 \end{matrix} & \begin{matrix} R_{4,1}^2, R_{4,1}^3 \\ R_{4,1}^5 \end{matrix} & R_{4,1}^1 & \begin{matrix} R_{5,1}^1, R_{5,1}^2, R_{5,1}^3, R_{6,1}^1, R_{6,1}^2, R_{6,1}^3, R_{7,1}^1, R_{7,1}^2, R_{7,1}^3 \\ R_{5,1}^4, R_{5,1}^5, R_{6,1}^4, R_{6,1}^5, R_{7,1}^4, R_{7,1}^5 \end{matrix} & \begin{matrix} R_{6,1}^1, R_{6,1}^2, R_{6,1}^3, R_{7,1}^1, R_{7,1}^2, R_{7,1}^3 \\ R_{6,1}^4, R_{6,1}^5, R_{7,1}^4, R_{7,1}^5 \end{matrix} & \begin{matrix} 0 \\ 0 \\ 0 \\ 0 \end{matrix} & \begin{matrix} 0 \\ 0 \\ 0 \\ 0 \end{matrix} & \begin{matrix} 0 \\ 0 \\ 0 \\ 0 \end{matrix} & \vec{R} \end{bmatrix}$$

Figure 8 The hexacopter's dynamic residual terms vector is developed by combining the chains' dynamic residual terms vectors shown in Figure 5.

Since the desired trajectory is determined such that the axes of coordinate system $x_2y_2z_2$ align with the axes of coordinate system $e_ie_ne_b$, we can equate Eqs. (24) and (25) as follows:

$$\begin{aligned}
\theta_{-1}^d &= \tan^{-1} \left(-\frac{\gamma_3}{\gamma_1} \right) \\
\theta_0^d &= \sin^{-1} \gamma_2 \\
\theta_1^d &= \frac{\pi}{3} + \tan^{-1} \left(-\frac{\beta_2}{\alpha_2} \right) \quad (26)
\end{aligned}$$

The superscript d in Eq. (26) is used to emphasize the desired values achieved for the angles of the hexacopter. Thus, all the desired angles that yield the defined orientation for this robotic system are determined. Of course, as emphasized in Section 2, some of these angles should always have a constant value ($\theta_2^d = -\frac{2\pi}{3}$, $\theta_3^d = -\frac{\pi}{3}$, $\theta_4^d = 0$, $\theta_5^d = \frac{\pi}{3}$, $\theta_6^d = \frac{2\pi}{3}$). It is vital to stress that $\theta_2^d = -\frac{2\pi}{3}$ was used in the derivation of Eq. (26).

In the proceeding sections, an expression for the generalized coordinates related to the position of the first motor, i.e., X_{O_1} , Y_{O_1} , and Z_{O_1} , in terms of the desired trajectory of the hexacopter's center should be obtained. Using equation ${}^0\vec{r}_{O_2} = {}^0\vec{r}_{O_1} + {}^{X_0Y_0Z_0}R_{x_1y_1z_1} \{ l_1 \ 0 \ 0 \}^T$, the

components of this point's desired position relative to the inertial coordinate system are derived as follows:

$$\begin{aligned}
X_{O_1}^d &= X_{O_2}^d - l_1 (\sin \theta_{-1}^d \sin \theta_1^d - \cos \theta_{-1}^d \sin \theta_0^d \cos \theta_1^d) \\
Y_{O_1}^d &= Y_{O_2}^d - l_1 \cos \theta_0^d \cos \theta_1^d \\
Z_{O_1}^d &= Z_{O_2}^d - l_1 (\cos \theta_{-1}^d \sin \theta_1^d + \sin \theta_{-1}^d \sin \theta_0^d \cos \theta_1^d) \quad (27)
\end{aligned}$$

where l_1 denotes the length of the first arm of the hexacopter. Thus, all generalized coordinates of the system, including the desired angles and the desired position of the first motor, are determined in terms of the parametric equations of the hexacopter's center.

5. Solving the hexacopter's motion equations

Now, having the desired path of the system, we are seeking to calculate the thrust forces generated by the six motors installed on the hexacopter to track this path. To achieve this goal, we present the first 11 equations of Eq. (19) as follows:

$$A \ddot{\vec{q}} + B \vec{\tau}' = \vec{R} + \Psi \vec{F} \quad (28)$$

In which the matrices A , B , Ψ , and vector \vec{R} are introduced in Figure 7 through 9. On the other hand, the generalized coordinate vector \vec{q} , the active force vector

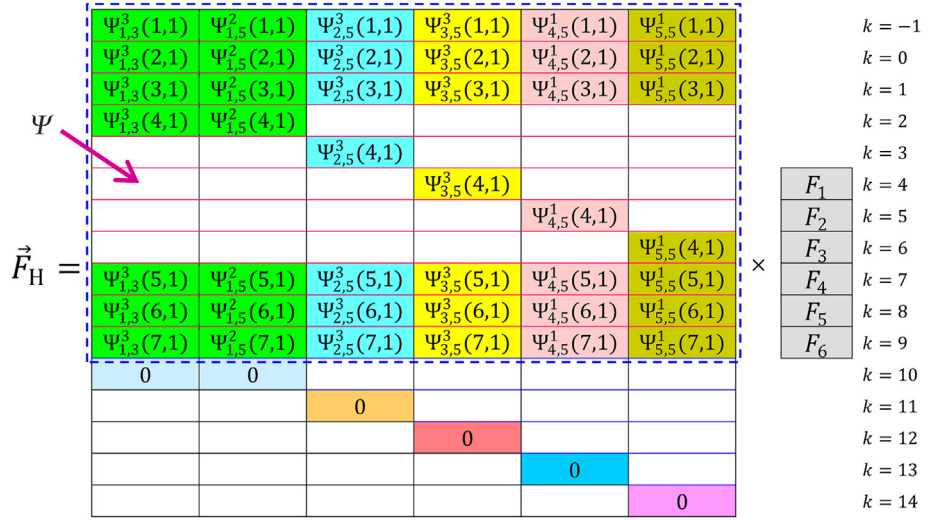


Figure 9 The hexacopter's generalized forces vector is developed by combining the chains' generalized forces vectors shown in Figure 5.

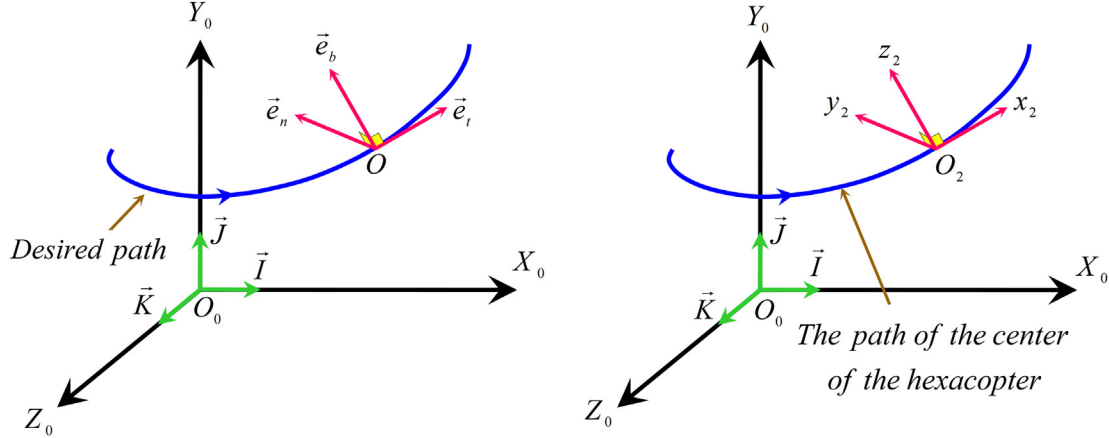


Figure 10 The desired path for the center of the hexacopter is such that the axes of the coordinate system $x_2y_2z_2$ are aligned consistently with the axes of the coordinate system $e_te_ne_b$.

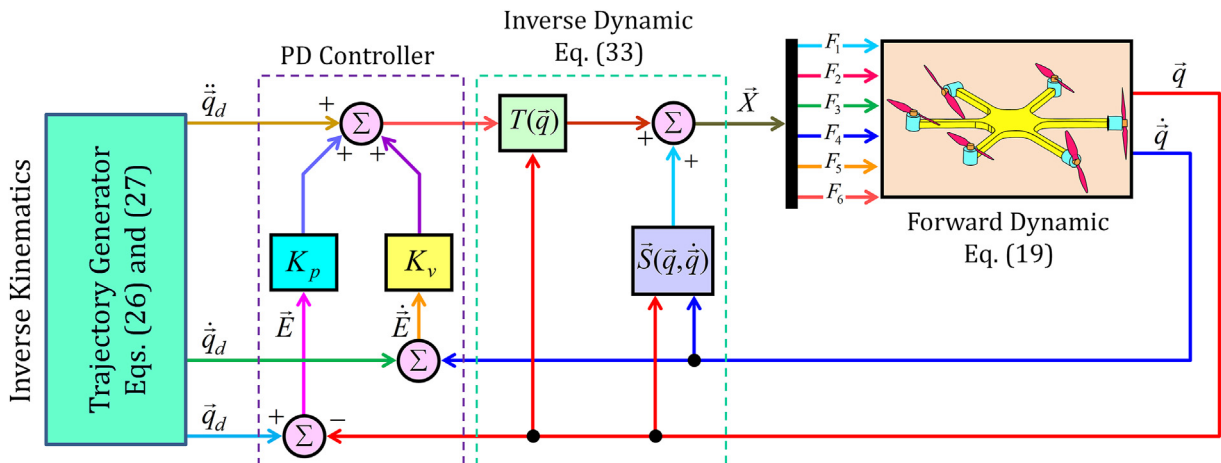


Figure 11 The block diagram for simulating the motion equations of the hexacopter examined in this paper.

\vec{F} , and the constraint torque vector $\vec{\tau}'$ are defined as follows:

$$\vec{q} = \{ \theta_{-1} \ \theta_0 \ \theta_1 \ \theta_2 \ \theta_3 \ \theta_4 \ \theta_5 \ \theta_6 \ X_{O_1} \ Y_{O_1} \ Z_{O_1} \}^T$$

$$\vec{\tau}' = \{ \tau'_1 \ \tau'_2 \ \tau'_3 \ \tau'_4 \ \tau'_5 \}^T$$

$$\vec{F} = \{ F_1 \ F_2 \ F_3 \ F_4 \ F_5 \ F_6 \}^T \quad (29)$$

By rearranging Eq. (28) to place the unknown variables on the left side and the known variables on the right side, we obtain:

$$P\vec{X} = \vec{R} - A\ddot{\vec{q}} \quad (30)$$

where

$$P = [B_{11 \times 5} \ -\Psi_{11 \times 6}]_{11 \times 11} \quad (31)$$

$$\vec{X} = \{ \vec{\tau}'^T \ \vec{F}^T \}^T$$

Pre-multiplying matrix P^{-1} on both sides of Eq. (30) yields the vector \vec{X} , which represents the unknown variables as follows:

$$\vec{X} = \vec{S} + T\ddot{\vec{q}} \quad (32)$$

where $\vec{S} = P^{-1}\vec{R}$, and $T = -P^{-1}A$. Here, it is necessary to discuss an important issue. As previously stated, in order to obtain the vector of unknown variables \vec{X} , the inverse of the matrix P should be calculated. This can only happen if this 11×11 matrix is invertible. This matrix, as observed, consists of two separate components. One, denoted as B , is composed of fixed entries, and we cannot manipulate its elements (please see Figure 7). The second part is matrix Ψ , where its columns were acquired according to Eq. (15) as $\vec{\Psi}_{j,i}^k = J_{j,i}^{T0} R_{j,i} \vec{\vartheta}^k$. We observed that the motors' thrust force aligns with the $\vec{\vartheta}^k$ vector. Therefore, it is important to design the motor arrangement at each arm's end so that the P matrix becomes full-rank and, consequently, invertible. Figure 1 illustrates three different configurations for installing the motors at the end of each arm (Installing the motor to generate the thrust force aligned with the arm's x -axis, y -axis, or z -axis). On the other hand, since the hexacopter studied in this article consists of six arms, there are $3^6 = 729$ possible arrangements for motor installation. After analyzing all these 729 states, the authors concluded that only 116 states result in a non-singular condition. In this work, one of these states for dynamic modeling was selected, as shown in Figure 1.

Here, another important issue arises. The solution of Eq. (32) determines the vector \vec{X} , which consists of the constraint torques and the thrust forces generated by the motors. The robot initially follows the defined desired

trajectory by applying the thrust forces to the system through the direct dynamic process, but gradually deviates from it over time. Indeed, numerical integration errors lead to significant deviations between the obtained and desired results, as these errors accumulate over time. Thus, we utilize the subsequent *PD* control law [56]:

$$\vec{X} = \vec{S} + T \left(\ddot{\vec{q}}_d + K_v \dot{\vec{E}} + K_p \vec{E} \right) \quad (33)$$

where the error vector \vec{E} is presented as the difference between the desired and actual values as follows:

$$\vec{E} = \vec{q}_d - \vec{q} \quad (34)$$

By equating Eqs. (32) and (33), the error equation can be obtained in terms of the control gain matrices K_v and K_p as follows:

$$\ddot{\vec{E}} + K_v \dot{\vec{E}} + K_p \vec{E} = \vec{0} \quad (35)$$

To achieve the fastest convergence of the error differential equations to zero, it is necessary to select the control gain matrices that result in critical damping. So, we have $K_v = 2\sqrt{K_p}$.

6. Presenting the results of the hexacopter simulation

In this section, the results of simulating the motion equations are discussed. Figure 11 illustrates the block diagram for the entire simulation procedure. As displayed in this figure, to generate the desired generalized coordinates using Eqs. (26) and (27), the trajectory of the hexacopter's center (i.e., O_2) should be known. In this paper, the following spiral path, whose cross-sectional area along Y_0 is continuously decreasing, has been selected.

$$\begin{aligned} X_{O_2}^d &= 4e^{-0.05t} \cos t \\ Y_{O_2}^d &= e^{0.05t} \\ Z_{O_2}^d &= 4e^{-0.05t} \sin t \end{aligned} \quad (36)$$

On the other hand, based on this figure, the physical parameters of the system are also required. In this article, it is assumed that each arm of the hexacopter has a length of $l_i = 0.5$ m, $i = 1, \dots, 6$, and mass per unit length of $\mu_i = 1$ kg/m, $i = 1, \dots, 6$. Additionally, the values of $K_p = 225 \times I_{11 \times 11}$ and $K_v = 30 \times I_{11 \times 11}$ are selected for the control gain matrices. Furthermore, the initial conditions for starting the computer simulation match exactly the system's desired initial conditions obtained from solving the inverse kinematics problem. These initial conditions for this robotic system are as follows:

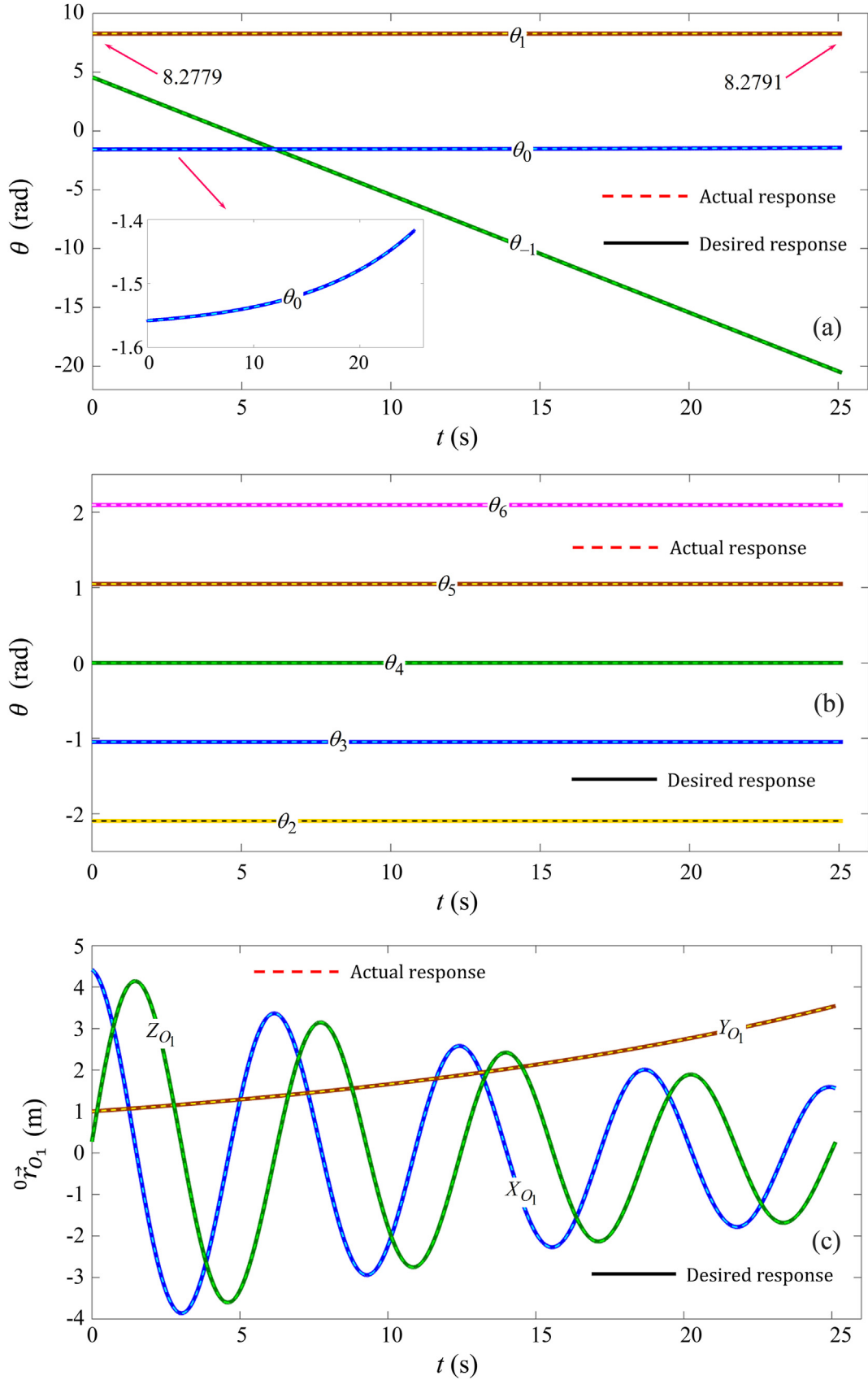


Figure 12 Generalized coordinates of the system in both the desired and actual states, including the angular positions of joints ((a) and (b)) as well as the position of joint O_1 relative to the inertial coordinate system (c).

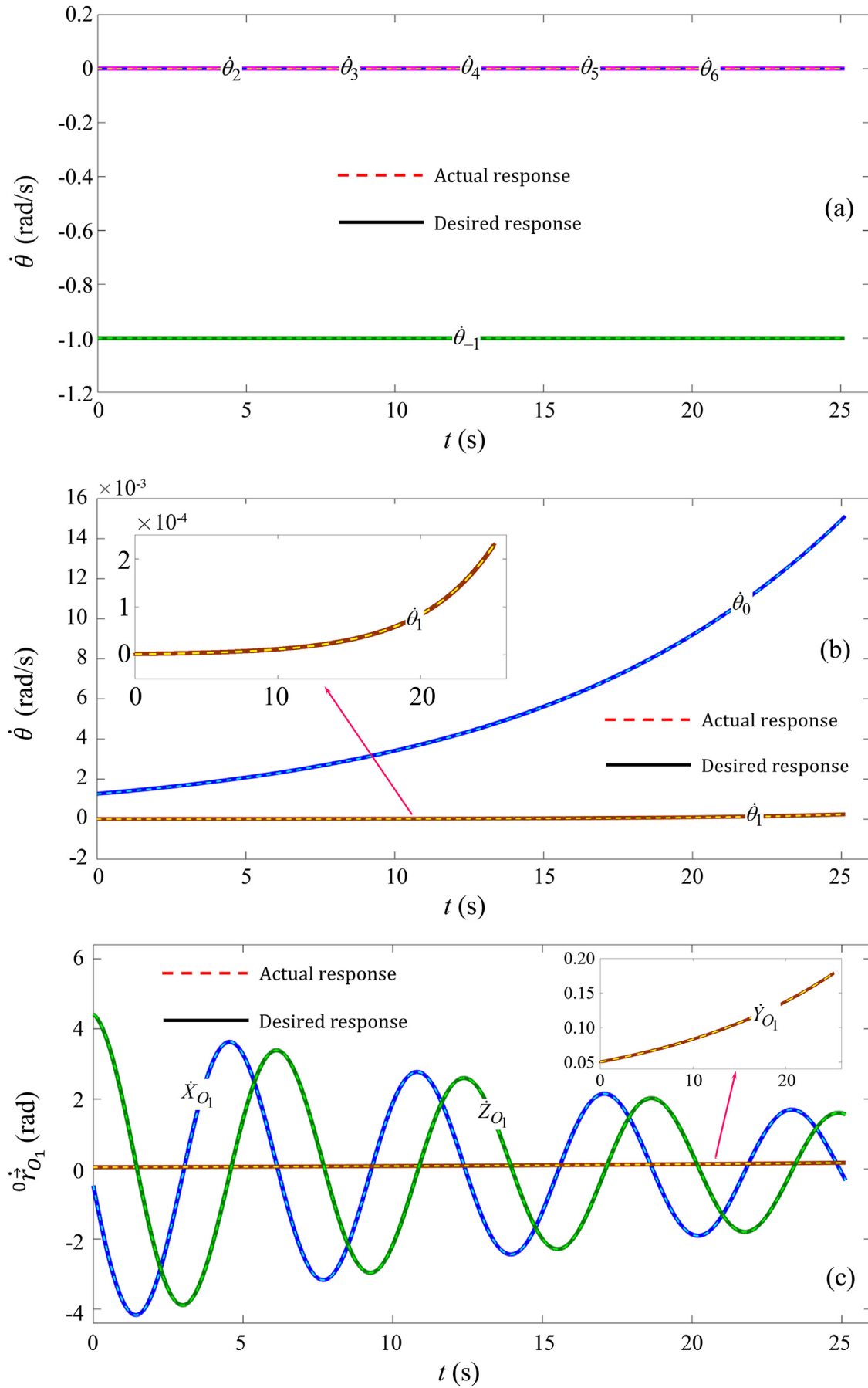


Figure 13 Generalized velocities of the system in both the desired and actual states, including the angular velocities of joints ((a) and (b)) as well as the velocity of joint O_1 relative to the inertial coordinate system (c)).

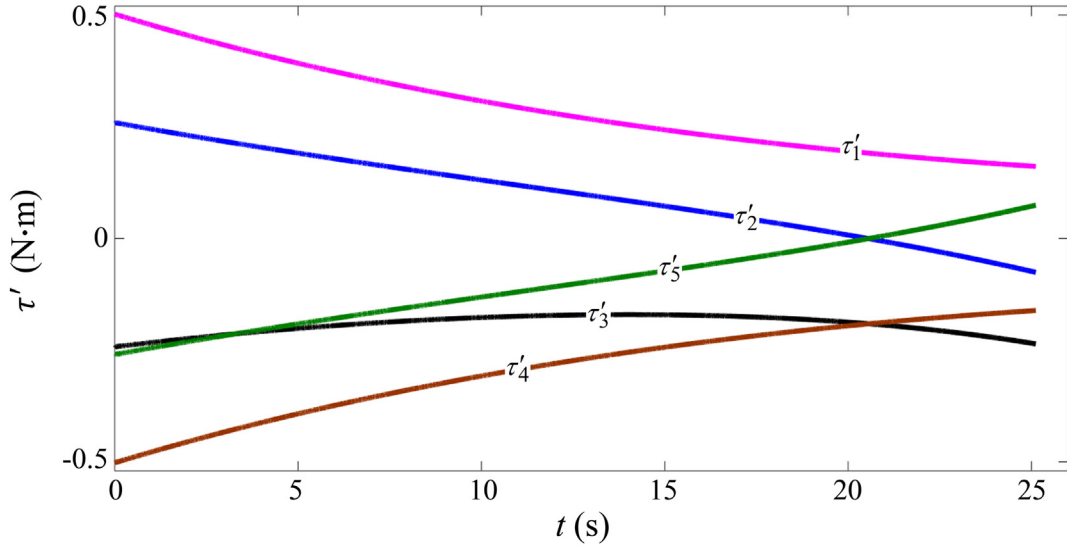


Figure 14 Constraint torques applied to each arm of the hexacopter.

$$\vec{q}|_{t=0} = \vec{q}^d|_{t=0} = \begin{bmatrix} 4.5628 \text{ rad} & -1.5583 \text{ rad} \\ 8.2779 \text{ rad} & -2.0944 \text{ rad} \\ -1.0472 \text{ rad} & 0.0000 \text{ rad} \\ 1.0472 \text{ rad} & 2.0944 \text{ rad} \\ 4.4200 \text{ m} & 1.0026 \text{ m} \\ 0.2713 \text{ m} \end{bmatrix}^T$$

$$\dot{\vec{q}}|_{t=0} = \dot{\vec{q}}^d|_{t=0} = \begin{bmatrix} -1.0000 \text{ rad/s} & 0.0013 \text{ rad/s} \\ 0.0000 \text{ rad/s} & 0.0000 \text{ rad/s} \\ 0 \text{ rad/s} & 0 \text{ rad/s} \\ 0 \text{ rad/s} & 0 \text{ rad/s} \\ -0.4715 \text{ m/s} & 0.0503 \text{ m/s} \\ 4.4200 \text{ m/s} \end{bmatrix}^T$$

$$\int \int \tau'_i dt dt|_{t=0} = 0 \text{ N}\cdot\text{m}\cdot\text{s}^2; \quad i=1, \dots, 5$$

$$\int \tau'_i dt|_{t=0} = 0 \text{ N}\cdot\text{m}\cdot\text{s}; \quad i=1, \dots, 5 \quad (37)$$

The results of the simulation are presented in the following figures. In [Figure 12](#), the angular positions of unconstrained joints, constrained joints, and the position of joint O_1 relative to the inertial coordinate system $X_0Y_0Z_0$ are presented in sections (a), (c), and (c) of this figure, respectively. According to this figure, it can be concluded that the unconstrained joints, where their variations lead to a change in the hexacopter's orientation, precisely follow the defined desired orientation. Also, the constrained joints θ_2 to θ_6 , where the consistency of these angles results in the coherence and integrity of the hexacopter, can be easily

concluded from this figure. The harmonic variations of the X_{O_1} and Z_{O_1} components results from the spiral motion of the hexacopter in the $X_0O_1Z_0$ plane, while the gradual increase of Y_{O_1} is the result of the ascent of the hexacopter in the Y_0 direction. Another point that should be mentioned is the way the angle θ_0 changes. Although it appears that the value of this angle remains constant throughout the hexacopter maneuver, zooming in on this plot reveals minor fluctuations of ten degrees ($-1.558 \text{ rad} < \theta_0 < -1.417 \text{ rad}$). Meanwhile, the angle θ_1 changes only 0.0664° during this time period ($8.2779 \text{ rad} < \theta_1 < 8.2791 \text{ rad}$).

In [Figure 13](#), the generalized velocities of the system, which are essentially the derivatives of the generalized coordinates with respect to time, are presented. In section (a) of this figure, the velocities of the constrained joints of this robotic system are plotted, which, as expected, are all equal to $\dot{\theta}_i = 0 \text{ rad/s}; i = 2, \dots, 6$. In the same figure, the velocity of the unconstrained joint $\dot{\theta}_{-1}$ is depicted, which has a constant value of $\dot{\theta}_{-1} = -1 \text{ rad/s}$. The angular velocities of the other two unconstrained joints (i.e., $\dot{\theta}_0$ and $\dot{\theta}_1$) are plotted in section (b) of this figure. As is observed in this section of [Figure 13](#), the order of the angular velocities for these two joints is very small, so that $\dot{\theta}_0$ is the order of 10^{-3} and $\dot{\theta}_1$ is the order of 10^{-4} . Furthermore, the velocity components of joint O_1 (i.e., \dot{X}_{O_1} , \dot{Y}_{O_1} , and \dot{Z}_{O_1}) are presented in section (c) of this figure. Here, as expected, the components \dot{X}_{O_1} and \dot{Z}_{O_1} exhibit harmonic variations, while \dot{Y}_{O_1} changes exponentially with a very gentle slope. It is essential to note a point regarding the system response presented in [Figures 12 and 13](#). The perfect match between the desired response obtained from solving the inverse kinematics problem, and the actual system response resulting from the application of control inputs (F_1, F_2, F_3, F_4, F_5 , and F_6) to the system and

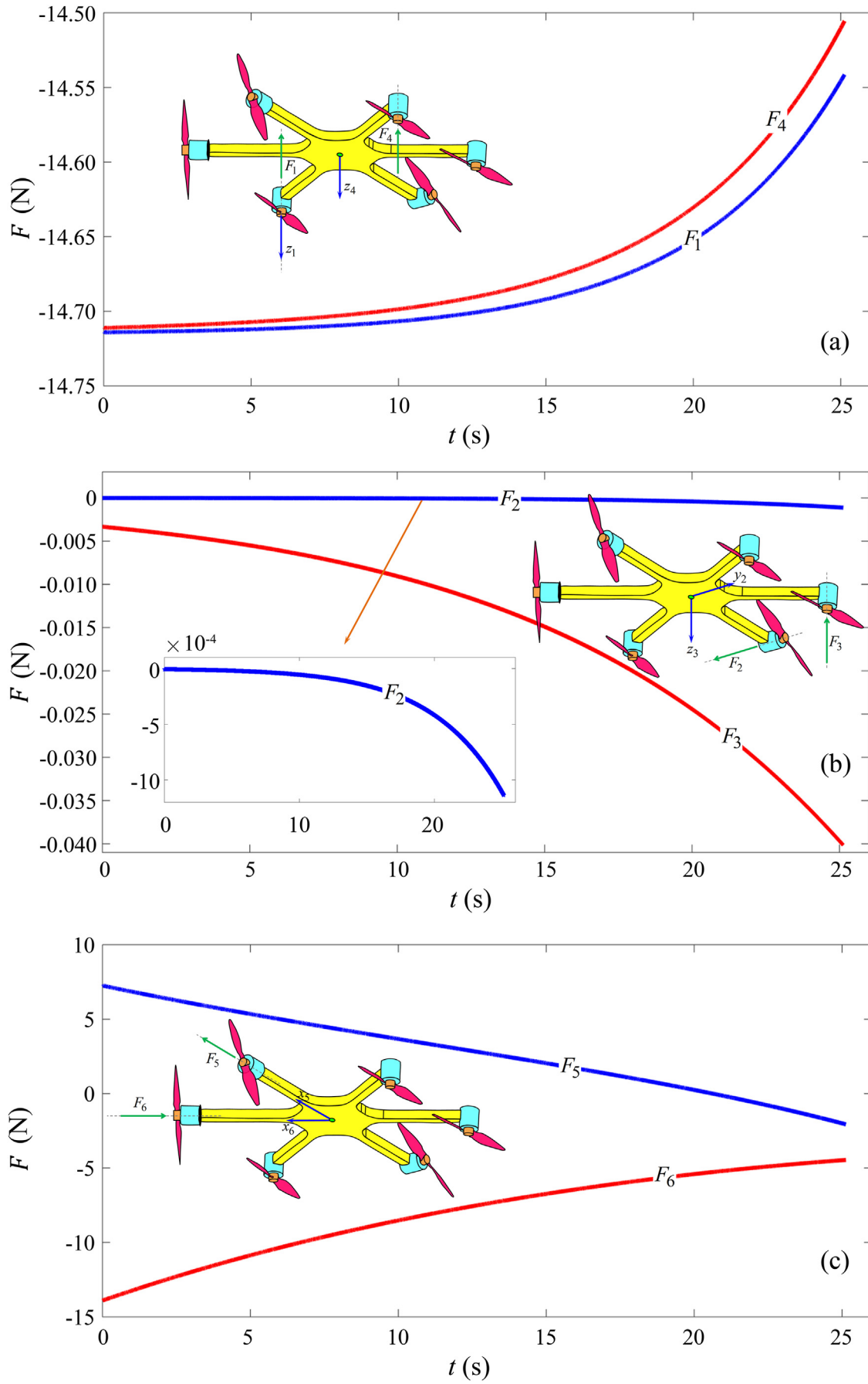


Figure 15 Thrust forces created by six motors installed at the end of the hexacopter's arms.

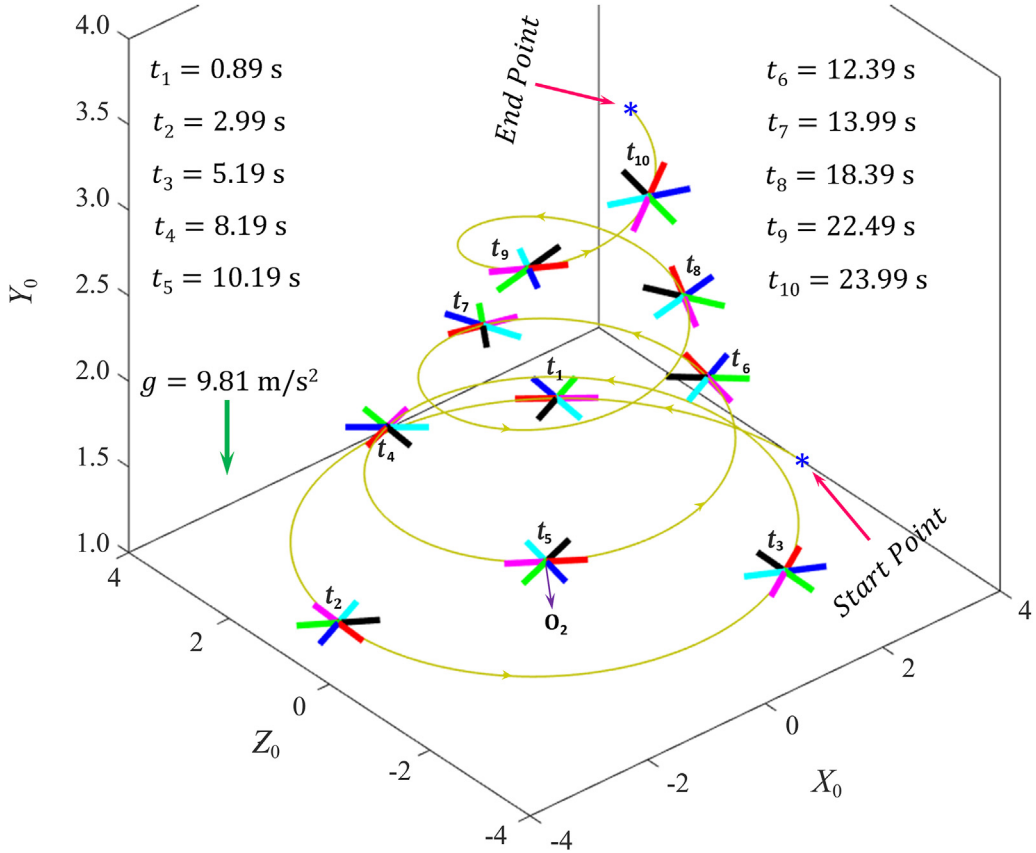


Figure 16 Simulation of the hexacopter’s movement along the desired path.

solving the direct dynamics problem indicates that the control system employed in this paper, despite its simplicity, exhibits satisfactory performance in tracking the desired trajectory.

As concluded from Eq. (37) and Figure 7, the constraint torques’ first and second integrals also appear in the form of generalized coordinates and generalized velocities. Thus, by performing numerical differentiations on the obtained values for $\int \tau'_i dt$; $i = 1, \dots, 5$, one can determine the constraint torques during the movement of the robot (Figure 14). These constraint torques refer to the torques applied to each arm of the hexacopter by the robot platform. Therefore, the platform of this robotic system must possess sufficient resilience to withstand these constraint torques, ensuring that it maintains its structural integrity and consistency during motion.

Figure 15 shows the most important result of this robotic system’s simulation: the thrust force generated by each motor. Section (a) of this figure depicts the thrust forces produced by the first and fourth motors. Since the weight of the hexacopter is equal to $W = mg = 6 \times 0.5 \times 1 \times 9.81 = 29.43$ N, it can be concluded that these two motors carry the majority of this weight. However, according to section (b) of this figure, the third motor, which has the same arrangement as the first and fourth motors, only supports a small portion of this weight. Upon revisiting section (b) of Figure 15, it becomes apparent that the

thrust force produced by the second motor is very negligible and of the order 10^{-4} . This issue can be justified when the very small changes in angle θ_1 are also considered. As was mentioned earlier, the robot’s weight is carried by the thrust forces created by the first, third, and fourth motors. The second motor is solely responsible for adjusting the hexacopter’s orientation according to the desired direction, which can be accomplished by exerting a minute amount of force by this motor. Part (c) of this figure presents the thrust forces produced by the fifth and sixth motors. As seen in this figure, the magnitude of these two forces is of order 10^1 . Indeed, these two forces are responsible for producing the spiral motion of the hexacopter within the $X_0O_2Z_0$ plane. To accomplish this objective, the magnitudes of these two forces must be unequal. This will result in creating a rotational couple while simultaneously generating the necessary force for movement within this plane.

Finally, to better understand this robotic system’s motion, we preferred to illustrate the movement of the entire system with respect to the inertial coordinate system rather than plotting the time response of each joint’s position. Figure 16 shows the robot’s desired trajectory as well as its position at ten different times. The hexacopter initiates its motion at position $X_{O_2} = 4$ m, $Y_{O_2} = 1$ m, $Z_{O_2} = 0$ m and, after $t = 8\pi$ s, terminates at the ultimate position $X_{O_2} = 1.1384$ m, $Y_{O_2} = 3.5136$ m, $Z_{O_2} = 0$ m. This

figure shows how the center of the hexacopter, i.e., O_2 , moves on the defined desired path. Another important point in this figure is this aerial robot's orientation, which matches the desired orientation defined in Section 4. This means that the second arm of the hexacopter (red link) is always tangent to the path of motion. This is the desired orientation, whose mathematical formulas were presented earlier in Eq. (26). This figure also demonstrates the desired performance of the *PD* controller in tracking the desired path despite the simple structure of this controller.

7. Conclusion

This study presents the process of deriving the motion equations for hexacopter robots using a standard methodology. The method used in this study allows for modeling any form of aerial robots of this type, regardless of the number of arms or their arrangement relative to each other. The entire process of extracting the motion equations of this robotic system, including the inertia matrix, the vectors of the dynamic residual term, and the generalized force vectors, was carried out in a completely automatic and systematic manner. In extracting the motion equations of this aerial robot, the constraints governing it, namely the non-rotation of the hexacopter arms relative to each other, were effectively modeled. The most important feature of the hexacopter examined in this research is its ability to execute complex maneuvers with the minimum number of actuators. In fact, the motors installed on the six arms of this robotic system, if properly arranged to ensure robot controllability, enable us to reach any point in space with any desired orientation. To demonstrate this issue, a relatively complex spatial path was tracked. The simulation results demonstrated the robot's ability to track the defined path and achieve the desired orientation.

As we know, for determining the proper dimension of robot's frame and using the right type of motors with optimal torques at the end of each arm, the kinematic and dynamic analysis of such robots becomes inevitable. Therefore, the motion equations of aerial robots, in their most general forms, were presented in this paper in the context of computer algorithms. This method enables the designers of multi-rotor UAVs to input a series of initial data (like those used in Section 6 for computer simulation) and determine the torques needed by the motors of their considered robot. Another characteristic of the presented formulation is their recursive nature, as they are able to perform the necessary kinematic and dynamic computations in the shortest possible time and using the least number of mathematical operations.

One of the research's flaws is that the motors' mass was not considered in the dynamic modeling of this robotic system. Furthermore, the primary focus of this study was on dynamic modeling. Therefore, we didn't use a highly advanced control system to track the desired path. On the

other hand, installing a mechanical arm on the robot's platform significantly improves its ability to perform manipulation tasks. These considerations, along with manufacturing a hexacopter with the features mentioned in this paper for the purpose of comparing theoretical and experimental results, are all suggestions for future works.

Appendix A. Supplementary data

Supplementary data to this article can be found online at <https://doi.org/10.1016/j.jppr.2025.02.004>.

References

- [1] M. Allenspach, K. Bodie, M. Brunner, L. Rinsoz, Z. Taylor, M. Kamel, R. Siegwart, J. Nieto, Design and optimal control of micro-aerial vehicle for efficient omnidirectional flight, *Int. J. Robot Res.* 39 (2020) 1305–1325.
- [2] K. Bodie, Z. Taylor, M. Kamel, R. Siegwart, Towards efficient full pose omnidirectionality with overactuated MAVs, in: *International Symposium on Experimental Robotics*, Springer, Berlin, 2018.
- [3] P. Ramon-Soria, B. Arregui, A. Ollero, Grasp planning and visual servoing for an outdoors aerial dual manipulator, *Engineering* 6 (1) (2020) 77–88.
- [4] R. Urban, M. Štroner, I. Kuric, The use of onboard uav gnss navigation data for area and volume calculation, *Acta Montan. Slovaca* 25 (2020) 361–374.
- [5] V. Stenclák, V. Tlach, I. Kuric, M. Bohušík, Z. Sagova, D. Wieček, Possibilities of implementing pre-trained feed-forward neural¹ networks in mobile robotics, *Transp. Res. Procedia* 74 (2023) 418–425.
- [6] G. Ducard, M. Hua, Wca : a new efficient nonlinear adaptive control allocation for planar hexacopters, *IEEE Access* 11 (2023) 37714–37748.
- [7] J. Zhang, D. Gu, C. Deng, B. Wen, Robust and adaptive backstepping control for hexacopter UAVs, *IEEE Access* 7 (2019) 163502–163514.
- [8] S. Omari, M. Hua, G. Ducard, T. Hamel, Hardware and software architecture for nonlinear control of multirotor helicopters, *IEEE ASME Trans. Mechatron.* 18 (6) (2013) 1724–1736.
- [9] J. Park, N. Cho, Collision avoidance of hexacopter UAV based on LiDAR data in dynamic environment, *Remote Sens.* 12 (6) (2020) 975.
- [10] H. Heidari, M. Saska, Collision-free trajectory planning of multi-rotor UAVs in a wind condition based on modified potential field, *Mech. Mach. Theor.* 156 (2021) 104140.
- [11] B. Ghalamchi, Z. Jia, M.W. Mueller, Real-time vibration-based propeller fault diagnosis for multicopters, *IEEE ASME Trans. Mechatron.* 25 (1) (2020) 395–405.
- [12] P. Guo, K. Xu, H. Deng, H. Liu, X. Ding, Modeling and control for aerial manipulation based on center of inertia on SE(3), *Nonlinear Dyn.* 111 (2023) 369–389.
- [13] Y. Chen, G. Zhang, Y. Zhuang, H. Hu, Autonomous flight control for multi-rotor UAVs flying at low altitude, *IEEE Access* 7 (2019) 42614–42625.
- [14] M. Kamel, S. Verling, O. Elkhatabi, C. Sprecher, P. Wulkop, Z. Taylor, R. Siegwart, I. Gilitschenski, The voliro omniorientational hexacopter: an agile and maneuverable tilttable-rotor aerial vehicle, *IEEE Robot. Autom. Mag.* 25 (4) (2018) 34–44.
- [15] W. Ye, P. Zhang, H. Chang, A data-driven optimal time-delayed control approach and its application to aerial manipulators, *Control Eng. Pract.* 142 (2024) 105754.
- [16] J.M. Arizaga, A. Miranda-Moya, H. Castañeda, P. Castillo, Observer-based adaptive control for slung payload stabilization with a fully-actuated multirotor UAV, *ISA (Instrum. Soc. Am.) Trans.* (2024), <https://doi.org/10.1016/j.isatra.2024.02.015>.

- [17] H. Lee, H.J. Kim, Constraint-based cooperative control of multiple aerial manipulators for handling an unknown payload, *IEEE Trans. Ind. Inf.* 13 (6) (2017) 2780–2790.
- [18] P. Guo, K. Xu, H. Deng, H. Liu, X. Ding, Modeling and control of a hexacopter with a passive manipulator for aerial manipulation, *Complex & Intelligent Systems* 7 (2021) 3051–3065.
- [19] J.I. Giribet, R.S. Sanchez-Pena, A.S. Gherzin, Analysis and design of a tilted rotor hexacopter for fault tolerance, *IEEE Trans. Aero. Electron. Syst.* 52 (4) (2016) 1555–1567.
- [20] E.L. De Angelis, F. Giulietti, Stability and control issues of multirotor suspended load transportation: an analytical closed-form approach, *Aero. Sci. Technol.* 135 (2023) 108201.
- [21] J. Liang, H. Zhong, Y. Wang, Y. Chen, J. Mao, W. Wang, H. Zhang, Reference optimization-based compliant control for aerial pipeline inspection using a hexacopter with a robotic contact device, *IEEE ASME Trans. Mechatron.* (2024), <https://doi.org/10.1109/TMECH.2024.3361040>.
- [22] A.M. Shafei, H.R. Shafei, Dynamic modeling of tree-type robotic systems by combining 3×3 rotation and 4×4 transformation matrices, *Multibody Syst. Dyn.* 44 (4) (2018) 367–395.
- [23] V. Rezaei, A.M. Shafei, Dynamic analysis of flexible robotic manipulators constructed of functionally graded materials, *Iranian Journal of Science and Technology, Transactions of Mechanical Engineering* 43 (2019) 327–342.
- [24] A.M. Shafei, H.R. Shafei, Considering link flexibility in the dynamic synthesis of closed-loop mechanisms: a general approach, *J. Vib. Acoust.* 142 (2) (2020) 021004.
- [25] A.M. Shafei, H.R. Shafei, Dynamic behavior of flexible multiple links captured inside a closed space, *J. Comput. Nonlinear Dynam.* 11 (5) (2016) 051016.
- [26] A.M. Shafei, M.M. Riahi, The effects of mode shapes on the temporal response of flexible closed-loop linkages under the impulse excitation, *Mech. Syst. Signal Process.* 178 (2022) 109256.
- [27] A.M. Shafei, H. Mirzaeinejad, A novel recursive formulation for dynamic modeling and trajectory tracking control of multi-rigid-link robotic manipulators mounted on a mobile platform, *Proc. IME J. Syst. Control Eng.* 235 (7) (2021) 1204–1217.
- [28] A.M. Shafei, H. Mirzaeinejad, A general formulation for managing trajectory tracking in non-holonomic moving manipulators with rotary-sliding joints, *J. Intell. Rob. Syst.* 99 (2020) 729–746.
- [29] H.R. Shafei, M. Bahrami, H.A. Talebi, Trajectory tracking of an uncertain wheeled mobile robotic manipulator with a hybrid control approach, *J. Braz. Soc. Mech. Sci. Eng.* 42 (6) (2020) 1–26.
- [30] M.H. Korayem, A.M. Shafei, E. Seidi, Symbolic derivation of governing equations for dual-arm mobile manipulators used in fruit-picking and the pruning of tall trees, *Comput. Electron. Agric.* 105 (2014) 95–102.
- [31] A. Zahedi, A.M. Shafei, M. Shamsi, Application of hybrid robotic systems in crop harvesting: kinematic and dynamic analysis, *Comput. Electron. Agric.* 209 (2023) 107724.
- [32] A. Zahedi, A.M. Shafei, M. Shamsi, Kinetics of planar constrained robotic mechanisms with multiple closed loops: an experimental study, *Mech. Mach. Theor.* 183 (2023) 105250.
- [33] A. Zahedi, A.M. Shafei, M. Shamsi, On the dynamics of multi-closed-chain robotic mechanisms, *Int. J. Non Lin. Mech.* 147 (2022) 104241.
- [34] A.M. Shafei, Z. Sadeghi, The kinematics and kinetics of multi-closed-chain mechanisms in the impact and non-impact stages, *Meccanica* 57 (10) (2022) 2591–2608.
- [35] R. Fazel, A.M. Shafei, S.R. Nekoo, A new method for finding the proper initial conditions in passive locomotion of bipedal robotic systems, *Commun. Nonlinear Sci. Numer. Simulat.* 130 (2024) 107693.
- [36] R. Fazel, A.M. Shafei, S.R. Nekoo, Dynamic modeling and closed-loop control design for humanoid robotic systems: Gibbs–Appell formulation and SDRE approach, *Multibody Syst. Dyn.* 62 (1) (2024) 57–86, <https://doi.org/10.1007/s11044-023-09964-y>.
- [37] R. Fazel, A.M. Shafei, S.R. Nekoo, A general formulation for dynamic path planning and closed-loop tracking of multi-rigid-link bipedal robotic systems, *J. Braz. Soc. Mech. Sci. Eng.* 46 (1) (2024).
- [38] R. Fazel, A.M. Shafei, S.R. Nekoo, Kinematic analysis of flexible bipedal robotic systems, *Appl. Math. Mech.* 45 (5) (2024) 795–818.
- [39] M. Ahmadizadeh, A.M. Shafei, M. Fooladi, Dynamic modeling of closed-chain robotic manipulators in the presence of frictional dynamic forces: a planar case, *Mech. Base. Des. Struct. Mach.* 51 (8) (2023) 4347–4367.
- [40] M. Ahmadizadeh, A.M. Shafei, R. Jafari, *Int. J. Struct. Stabil. Dynam.* 21 (6) (2021) 2150075.
- [41] M. Ahmadizadeh, A.M. Shafei, M. Fooladi, Dynamic analysis of multiple inclined and frictional impact-contacts in multi-branch robotic systems, *Appl. Math. Model.* 91 (2021) 24–42.
- [42] M. Ahmadizadeh, A.M. Shafei, M. Fooladi, A recursive algorithm for dynamics of multiple frictionless impact-contacts in open-loop robotic mechanisms, *Mech. Mach. Theor.* 146 (2020) 103745.
- [43] M. Shirzadeh, A. Amirkhani, N. Tork, H. Taghavifar, Trajectory tracking of a quadrotor using a robust adaptive type-2 fuzzy neural controller optimized by cuckoo algorithm, *ISA Trans.* 114 (2021) 171–190.
- [44] L. Chen, Z. Liu, Q. Dang, W. Zhao, G. Wang, Robust trajectory tracking control for a quadrotor using recursive sliding mode control and nonlinear extended state observer, *Aero. Sci. Technol.* 128 (2022) 107749.
- [45] A. Ollero, M. Tognon, A. Suarez, D. Lee, A. Franchi, Past, present, and future of aerial robotic manipulators, *IEEE Trans. Robot.* 38 (1) (2022) 626–645.
- [46] P. Portillo, L.E. Garza-Castañón, L.I. Minchala-Avila, A. Vargas-Martinez, V.P. Cayuela, P. Payeur, Robust nonlinear trajectory controllers for a single-rotor UAV with particle swarm optimization tuning, *Machines* 11 (9) (2023) 870.
- [47] Ş. Yıldırım, N. Çabuk, V. Bakırçioğlu, Design and trajectory control of universal drone system, *Measurement* 147 (2019) 106834.
- [48] J. Park, N. Cho, S. Lee, Reactive collision avoidance algorithm for UAV using bounding tube against multiple moving obstacles, *IEEE Access* 8 (2020) 218131–218144.
- [49] M.M. Ferdaus, M. Pratama, S.G. Anavatti, M.A. Garratt, Y. Pan, Generic evolving self-organizing neuro-fuzzy control of bio-inspired unmanned aerial vehicles, *IEEE Trans. Fuzzy Syst.* 28 (8) (2020) 1542–1556.
- [50] L.J. Colombo, J.I. Giribet, Learning-based fault-tolerant control for an hexarotor with model uncertainty, *IEEE Trans. Control Syst. Technol.* 32 (2) (2024) 672–679.
- [51] J.A. Ricardo Jr., D.A. Santos, Smooth second-order sliding mode control for fully actuated multirotor aerial vehicles, *ISA (Instrum. Soc. Am.) Trans.* 129 (2022) 169–178.
- [52] A.M. Shafei, H. R. Shafei, A systematic method for the hybrid dynamic modeling of open kinematic chains confined in a closed environment, *Multibody Syst. Dyn.* 38 (1) (2016) 21–42.
- [53] A.M. Shafei, H.R. Shafei, Planar multibranch open-loop robotic manipulators subjected to ground collision, *J. Comput. Nonlinear Dynam.* 12 (6) (2017) 061003.
- [54] A.M. Shafei, H.R. Shafei, Dynamic modeling of planar closed-chain robotic manipulators in flight and impact phases, *Mech. Mach. Theor.* 126 (2018) 141–154.
- [55] M.H. Korayem, A.M. Shafei, Motion equations proper for forward dynamics of robotic manipulator with flexible links by using recursive Gibbs–Appell formulation, *Scientia Iranica Transaction b-Mechanical Engineering* 16 (6) (2009) 479–495.
- [56] H.R. Shafei, M. Bahrami, H.A. Talebi, Disturbance observer-based two-Layer control strategy design to deal with both matched and mismatched uncertainties, *Int. J. Robust Nonlinear Control* 31 (5) (2021) 1640–1656.